Université de Montréal

Modification of Microfibrillated Cellulose Foams by Atmospheric-Pressure Plasmas

Par

Louis-Félix Meunier

Département de physique, Faculté des Arts et des Sciences

Mémoire présenté en vue de l'obtention du grade de maîtrise

en physique, option plasma cheminement international

Mois et année du dépôt initial août 2020

Université de Montréal

Département de physique, Faculté des Arts et des Sciences

Ce mémoire intitulé

Modification of Microfibrillated Cellulose Foams by Atmospheric-Pressure Plasmas

Présenté par

Louis-Félix Meunier

A été évalué(e) par un jury composé des personnes suivantes

Ahmad Hamdan
Président-rapporteur

Luc Stafford
Directeur de recherche

Nicolas Naudé
Codirecteur

Joëlle Margot
Membre du jury

Résumé

Le traitement de différents polymères issus de sources renouvelables est, depuis relativement récemment, un domaine de très fort intérêt dans les communautés scientifiques. Ce travail aborde le traitement de mousses de microfibrille de cellulose, issues de biomasses forestières, dans des décharges à barrière diélectrique dans l'hélium à la pression atmosphérique. Lorsque la mousse occupe l'entièreté de l'espace inter-électrodes, nous avons montré que la décharge s'amorce et se propage à travers la mousse. L'effet de dégazer la mousse avant le traitement par plasma s'avère aussi bénéfique à la production de décharge de type « homogène ». En effet, en situation dégazée, la décharge à 60 kHz révèle une caractéristique « homogène » tandis qu'à 10 kHz elle devient filamentaire. Toutefois, nettement moins de dommage sont observés sur la mousse sujette à une décharge à 10 kHz par rapport à celle à 60 kHz. En situations non dégazées, le relâchement d'espèces issues de l'air ambiant lors de l'enclenchement de la décharge augmente considérablement la puissance injectée et dissipée dans le plasma, générant plus de dommage qu'en conditions dégazées. Ces connaissances ont ensuite été appliquées à la modification des mousses à l'aide d'un précurseur d'hexaméthyldisiloxane pour ajuster leurs mouillabilités à l'eau et à l'huile. Lorsque la mousse occupait tout l'espace inter-électrodes, le régime de décharge filamentaire produit des dépôts très inhomogènes, bien souvent localisés au voisinage des régions endommagées. Au contraire, lorsque la mousse n'occupe qu'une partie du volume inter-électrodes, une décharge homogène a été observée, induisant une défibrillation des fibres cellulosiques. Ces conditions mènent néanmoins à des surfaces hydrophobes sur les surfaces supérieure et inférieure des mousses, tout en maintenant leur caractéristique oléophile. Ces travaux semblent donc prometteurs pour la séparation efficace d'huile des eaux usées à partir de matériaux verts, biodégradables, et renouvelables.

Mots-clés : Matériaux cellulosiques, Interaction plasma-cellulose, décharge à barrière diélectrique, diagnostics optique et électriques, dépôt plasma, hydrophobicité, oléophilicité, adsorption sélective, dégazage, pression atmosphérique.

Abstract

The treatment of different polymers issued from renewable sources has recently become of high interest in today's scientific community. This work focused on the treatment of microfibrillated cellulosic foams, issued from wood biomass, in an atmospheric pressure dielectric barrier discharge in helium. When foams occupied all of gas gap volume, we demonstrated that the discharge ignites and propagates through the foams. The act of outgassing before plasma treatment has also been shown to be highly beneficial to the production of homogeneous glow-like discharges. Indeed, it was found that, in outgassed conditions, discharges occurring at a frequency of 60 kHz were glow-like, while those at 10 kHz were filamentary. However, significantly less damage was observed on the foams subjected to a 10 kHz discharge as opposed to those subjected to a 60 kHz discharge. In non-outgassed situations, we have also shown that the release of oxidising species originating from ambient air upon plasma ignition considerably increased injected and dissipated power in the plasma, in turn producing more damage than in outgassed conditions. This knowledge was then applied to the modification of these foams using a hexamethyldisiloxane precursor for plasma deposition to adjust their wettability to water and to oil. When foams occupied all of gas gap volume, the discharge regime was filamentary, and produced inhomogeneous coating, often very localised around damaged regions. When foams took up only a portion of gas gap volume, a homogeneous glow-like discharge was observed, inducing defibrillation of the cellulosic fibers. These conditions produced hydrophobicity on both the top and bottom surfaces of the foams, all while maintaining the foam's characteristic oleophilicity. This supports the idea of selective adsorption of oily wastewater using a green, biodegradable, and renewable cellulosic product.

Keywords : Cellulosic materials, plasma-cellulose interaction, dielectric barrier discharge, optical and electrical diagnostics, plasma deposition, hydrophobicity, oleophilicity, selective adsorption, outgassing, atmospheric pressure.

Table des matières

Résumé 5

Abstract 6

Table des matières 7

Liste des tableaux 11

Liste des figures 13

Liste des sigles et abréviations 17

Remerciements 21

Chapter 1 – Introduction 23

Chapter 2 – General Principles and Literature review 29

2.1 - Creation of non-thermal plasmas at atmospheric pressure 29

2.2 - Dielectric Barrier Discharges 29

2.3 - Breakdown and Discharge Regimes 31

2.4 - Dielectric Barrier Discharges in Presence of Complex Materials 35

2.4.1 - Substrate Outgassing 36

2.4.2 - Discharge Localisation Phenomenon 38

2.4.3 - Transport Phenomenon 41

2.5 - Dielectric Barrier Discharges for thin film deposition 42

2.6 – Summary 45

Chapter 3 – Results and Analysis 47

3.1 - Introduction 47

3.2 - Characterization of non-thermal dielectric barrier discharges at atmospheric pressure in presence of microfibrillated cellulosic foams 48

3.2.1 - Introduction 48
3.2.2 - Experimental details and data analysis methods 50
3.2.2.1 - Experimental setup 50
3.2.2.2 - Characterization Methods 52
3.2.3 - Experimental results and discussion 53
3.2.3.1 - Influence of the applied voltage frequency 53
3.2.3.2 - Influence of substrate outgassing 61
3.2.4 - Conclusion 67
3.2.5 - Acknowledgments 68
3.3 - Modification of Microfibrillated Cellulosic Foams in a Dielectric Barrier Discharge at Atmospheric Pressure 69
3.3.1 - Introduction 70
3.3.2 - Experimental details 72
3.3.2.1 - Sample Preparation 72
3.3.2.2 - Plasma Treatment 72
3.3.2.3 - Surface Morphology and Chemistry 74
3.3.2.3 - Contact Angle Measurements 74
3.3.3 - Experimental results and discussion 75
3.3.3.1 - Plasma Characterization 75
3.3.3.3 - Surface Chemical Characterization 81
3.3.3.4 - Water Contact Angle Measurements 84
3.3.3.5 - Oleophilicity Measurements 88
3.3.4 - Conclusion 90
3.3.5 - Acknowledgments 91

Chapter 4 – Conclusion and perspectives 93

Références bibliographiques 96

Liste des tableaux

Tableau 1. – Fundamental values of different discharge regimes in DBD configuration at atmospheric pressure [23] 34

Liste des figures

Figure 1. – Extraction of micro and nanofibrils from wood and plants [15].....25

Figure 2. – Principle behind a DBD plasma [1] – (A) Establishment of a first micro-discharge – (B) Attenuation of the first micro-discharge and beginning of a new one in a different position – (C) Polarity applied to system alternates – (D) Electrical schematic of the discharge [44].....30

Figure 3. – Characteristics of possible breakdown regimes in a DBD at atmospheric pressure. Gate width: 10 ns for (A), and 100 ns for (B) and (C) [1]. 31

Figure 4. – Townsend breakdown I-V curve [51] 33

Figure 5. – (Left) Optical image of the wood substrate treated with a N_2 filamentary discharge. (Right) Zoom of a burn on the wood substrate [56] 35

Figure 6. – Presence of N2, N2+, and O as a function of outgassing time [33] 37

Figure 7. – Influence of outgassing time on substrate [33] 38

Figure 8. – Spatial distribution of the helium plasma in presence of a (A) sugar maple substrate, (B) Douglas pine samples with tight and (C) wide late and early wood sections [34].....39

Figure 9. – Spatial evolution of the average electron temperature for the sugar maple and Douglas pine samples [34] 40

Figure 10. – Dynamics of the wetting process on sugar maple wood samples exposed to He and He/HMDSO (100 ppm) plasmas. Water contact angles from raw and freshly sanded sugar maple samples are also shown for comparison [51] 43

Figure 11. – Thin film coating percentage efficacy as a function of position on the substrate along the gas flow lines in plane-to-plane DBD [52].....44

.....45

Figure 12. – HMDSO growth rate profile over time along the gas flow on a surface through different power values [68].....45

Figure 13. – Schematic of the apparatus used for the production of DBDs in nominally high-purity pure helium with microfibrillated cellulosic (MFC) foams taking up the entirety of the gas gap…….....51

Figure 14. – I-Q-V measurements of a plane-to-plane DBD at 10 kHz with an outgassed MFC foam at different times over the total 60-min plasma treatment time: A) 2 min, B) 30 min, and C) 60 min……. 54
Figure 15. – I-Q-V measurements of a plane-to-plane DBD at 60 kHz with an outgassed MFC foam at different times over the total 60-min plasma treatment time: A) 2 min, B) 30 min, and C) 60 min…… 55
Figure 16. – Optical microscope images of the surface of the outgassed MFC foams after plasma treatment. A) Overall view of the surface; 10 kHz discharge. B) Close-up of a hole created by the presence of a filament; 10 kHz discharge (diameter: ≈ 0.4 mm, surface area: ≈ 0.1 mm^2). C) Overall view of the surface; 60 kHz discharge. D) Close-up of a hole created by the presence of a filament; 60 kHz discharge (diameter: ≈ 1.7 mm, surface area: ≈ 1.6 mm^2). 57
Figure 17. – ICCD image captures of the outgassed MFC foams subjected to a discharge at three different time intervals in order to observe potential time-based variations in light emissions patterns. For brevity, only the negative current alternance is shown (looking through the cathode). Similar results were obtained on the positive current alternance (looking through the anode). 10 kHz discharge – Gate width 45 µs – A) 5 min, B) 30 min, C) 60 min. 60 kHz discharge – Gate width 8 µs – D) 5 min, E) 30 min, F) 60 min. 58
Figure 18. – ICCD image of the MFC foam recorded through the side looking into the gas gap. For brevity, only the positive current alternance is shown (top electrode is anode and bottom electrode is cathode). Similar results were obtained on the negative current alternance (top electrode is cathode and bottom electrode is anode). 10 kHz discharge – Gate width 45 ns – A) discharge ignition point (low discharge current) and B) discharge propagation point (maximum discharge current). 60 kHz discharge – Gate width 16 ns – C) discharge ignition point (low discharge current) and D) discharge propagation point (maximum discharge current). 61
Figure 19. – I-Q-V curves of the non-outgassed MFC foams subjected to a 10 kHz discharge at A) 2 min and B) 60 min, and to a 60 kHz discharge at C) 2 min and D) 60 min. 62
Figure 20. – Power dissipated in the DBD as a function of plasma treatment time of both outgassed and non-outgassed MFC foams subjected to A) a 10 kHz discharge and B) a 60 kHz discharge……64

Figure 21. – Optical microscope images of the surface of the non-outgassed MFC foams after plasma treatment. A) Overall view of the surface; 10 kHz discharge. B) Close-up of a hole created by the presence of a filament; 10 kHz discharge (diameter: ≈ 1.2 mm, surface area: ≈ 0.6 mm^2). C) Overall view of the surface; 60 kHz discharge. D) Close-up of a hole created by the presence of a filament; 60 kHz discharge (diameter: ≈ 2.6 mm, surface area: ≈ 3.3 mm^2 65
Figure 22. – ICCD image captures of the non-outgassed MFC foams subjected to a discharge at two different time intervals in order to observe potential time-based variations in light emissions patterns. For brevity, only the negative current alternance is shown (looking through the cathode). 10 kHz discharge – Gate width 45 μs – A) 5 min, B) 60 min. 60 kHz discharge – Gate width 8 μs – C) 5 min, D) 60 min. 66
Figure 23. – Experimental setup used when (A) MFC foams occupy a portion of the gas gap volume and (B) MFC foams occupy the entirety of the gas gap volume. 73
Figure 24. – Current-voltage characteristics of a plane-to-plane He-HMDSO dielectric barrier discharge with an outgassed MFC foam taking up a portion of the gas gap volume (corresponds to Figure 23A) at (A) 2 min, (B) 30 min, and (C) 60 min of the 1-h total plasma treatment time. 76
Figure 25. – Current-voltage characteristics of a plane-to-plane He-HMDSO dielectric barrier discharge with an outgassed MFC foam taking up the whole gas gap volume (corresponds to Figure 23B) at (A) 2 min, (B) 30 min, and (C) 60 min of the 1-hour total plasma treatment time……. 77
Figure 26. – Pictures of the surfaces of the MFC foam. (A) Foam taking up a portion of the gas gap volume with no visible discolouration. (B) Foam taking up the entirety of the gas gap volume with visible yellow stained on its surface.....78
Figure 27. – (A)-(C) SEM images of the untreated MFC foams at different locations for various magnifications: X500 in (A), X2000 in (B) and X5000 in (C). (D)-(F) SEM images of the top side of the plasma-treated MFC foam taking up a portion of the gas gap at different locations for various magnifications: X500 in (D), X2000 in (E) and X5000 in (F). (G)-(I) SEM images of the bottom side of the plasma-treated MFC foam taking up a portion of the gas gap at different locations for various magnifications: X500 in (G), X2000 in (H) and X5000 in (I). (J)-(L) SEM image of the top side

of the plasma-treated MFC foam taking up the entirety of the gas gap at different locations for various magnifications: X500 in (J), X2000 in (K) and X5000 in (L). 79
Figure 28. – Mean C/O and Si/O ratios determined through EDS of different MFC foam plasma treatment configurations studied with a dashed line demonstrating the theoretical stoichiometric ratio for C/O (normalised to 1 for simplicity). Error bars indicate the standard deviation of the measurement.....82
Figure 29. – Mean WCA measurements and standard deviations (Error bars) at the top, and bottom surfaces of the MFC foams measured near the gas entry, the middle of the foam, and the gas exit. All values were recorded 45 s after droplet deposition. Data are shown for foam taking up a portion, and the entirety of the gas gap volume. 85
Figure 30. – The change of normalized water contact angle and water droplet volume over time after water droplet on a plasma-treated MFC foam (taking up a portion of the gas gap volume) and a plasma-treated silicon. The volume of water droplet settled on an untreated foam was also shown for comparison. 87
Figure 31. – Interaction of untreated MFC foam with either (A) water or (B) kerosene. Interaction of plasma-treated MFC foam (taking up a portion of the gas gap volume) with water and kerosene on (C) the top side and (D) the bottom side of the MFC foam. 89

Liste des sigles et abréviations

AC : Alternating Current

APGD : Atmospheric Pressure Glow Discharge

APTD : Atmospheric Pressure Townsend Discharge

ATR-FTIR : Attenuated Total Reflectance Fourier Transform Infrared Spectroscopy

CCTT : Centre Collégial de Transfert de Technologie

CNC : Cellulose Nanocrystalline

CNRS : Centre National de Recherche Scientifique

DBD : Dielectric Barrier Discharges

DC : Direct Current

EDS : Energy Dispersive x-ray Spectroscopy

FE : Field Emission

HMDSO : Hexamethyldisiloxane

ICCD : Charged Coupled Device

INPT : Institut Nationale Polytechnique Toulouse

ISPC24 : International Symposium on Plasma Chemistry 24

ITEGA : Institut de Technologie des Emballages et du Génie Alimentaire

ITO : Indium Tin Oxide

MFC : Microfibrillated Cellulosic

NFC : Nanofibrillated Cellulose

NSERC : National Science and Engineering Research Council

PPHARE : Physique des Plasma HAutement RÉactifs

PPP : Plasma Processes and Polymers

PSST : Plasma Sources Science and Technology

SEM : Scanning Electron Microscopy

slm : Standard Litre per Minute

WCA : Water Contact Angle

XPS : X-ray Photoelectron Spectroscopy

Ce mémoire est dédié à moi-même et à mes parents, à moi-même qui n'étais pas certain d'en être capable et à mes parents qui, eux, n'ont jamais douté.

Remerciements

Je tenais à dédier mes remerciements à plusieurs personnes, tout d'abord ma famille pour m'avoir appuyé pendant tout mon parcours, m'encourageant toujours à aller plus loin, et toujours prêt à m'aider si le chemin devenait un peu plus difficile. Je n'ose même pas imaginer où j'en serais rendu sans eux. Merci à tous mes ami(e)s de m'avoir écouté lorsque j'avais à me plaindre, d'avoir célébré avec moi lors de réussites, et aussi de m'avoir encouragé à continuer. Merci au groupe de recherche de Toulouse et de Montréal, ainsi qu'à mes directeurs de recherches, pour m'avoir aidé lors de culs-de-sac, et lorsque je perdais confiance. Je suis peut-être la personne qui a écrit les mots figurant dans ce document, mais ce travail n'aurait jamais été possible sans toutes les personnes qui m'ont appuyé pendant mon parcours, non seulement scolaire, mais de vie.

Chapter 1 – Introduction

For millennia, cellulose has been an integral part of cultural and societal development of the human species. An important part of our history is built around the technological advancements of cellulose, being used as wood, cotton, energy source, construction material, or part of clothing. Cellulose is an organic product offering incredibly interesting properties and has been shown to interact chemically and physically with other materials and media in very promising manners. It is a biopolymer that acts as the principle constituent of plant cell walls. It constitutes between 35% and 50% of all planetwide plant-based biomass, making it excessively widespread and accessible in large quantities [1].

These last few years, demands in renewable products have generated an increased interest in the potential valorisation of materials harvested from biomass. Amongst those, the synthesis of biodegradable products issued from cellulose could allow carbon-neutral or even carbon-negative processes to become carbon-positive despite their history. In fact, cellulose-based products currently offer a very promising alternative to current plastic-based polymers produced from polluting sources [2]. As humanity slowly comes to terms with its past and present shortcomings regarding the protection of our environment, governments worldwide are gradually implementing increasingly severe penalties and sanctions on polluting companies [3–6]. As a result, in order to prioritize industry revenue and the protection of our environment, the commercial market has incentive to find alternative materials to reduce its carbon footprint, and has chosen to lean towards cellulose. Since cellulose is an ecological, biocompatible, biodegradable, environmentally friendly material, and, mostly, inexhaustible, it is considered as an alternative biopolymer for direct application in many assembly lines [1,2,5–9]

.

Cellulose is presently used today in the forestry, paper, and textile domain to name a few but the one domain currently using the most cellulose-based materials is the composite materials sector. The cellulose currently used in todays industry are called first-generation cellulose [10]. Unfortunately, their marketing remains very difficult to this day [8,11–13]. Indeed, their high hygroscopicity and hydrophilicity (high sensibility of a substrate to humidity and aqueous solutions) of this first-generation cellulose greatly limits their potential uses and applications. For instance, it remains impossible for cellulose to replace any form of hydrophobic polymers, currently dominated by plastic-based polymers, a crucial milestone to conquer in cellulose based products if we are to protect our environment. Moreover, their tendency to expand when in presence of a liquid reduces even more their applications on an industrial scale. Many different areas of the scientific field have thus chosen to concentrate their efforts on the development and synthesis of a second-generation cellulose that can overcome most, if not all, the shortcomings of the first-generation cellulose [2]. This is, in part, what this project has set forth to solve.

For cellulose to become an integral part of the industrial sector, it must be a solid and durable material. A cellulose-based product already offers very interesting attributes in that regard, named crystalline nanocellulose (CNC). CNCs are responsible for granting plant cell walls their rigidity and solidity, and is known for being one of the most solid and rigid material that can be naturally found to this day. Extracted from wood and plants (Figure 1), these crystalline cellulose nanofibrils have a very small volumetric density, a high surface area, and easily modifiable surface properties thanks to their reactive hydroxyl chains at their axial extremities [2,5–9]. Moreover, certain tests have shown that CNCs possess a very high axial elasticity, vouching for their solidity and rigidity [9]. Some have even come forward to promote CNCs as the pioneer of nanotechnologies, as they can be used to generate products so small that the laws directing their mechanical behaviours are directed by physics at the nanoscale level. The field of possible applications of cellulose-based materials and nanomaterials grows every day, and has generated an explosive increase in scientific interest in their possible uses [10].

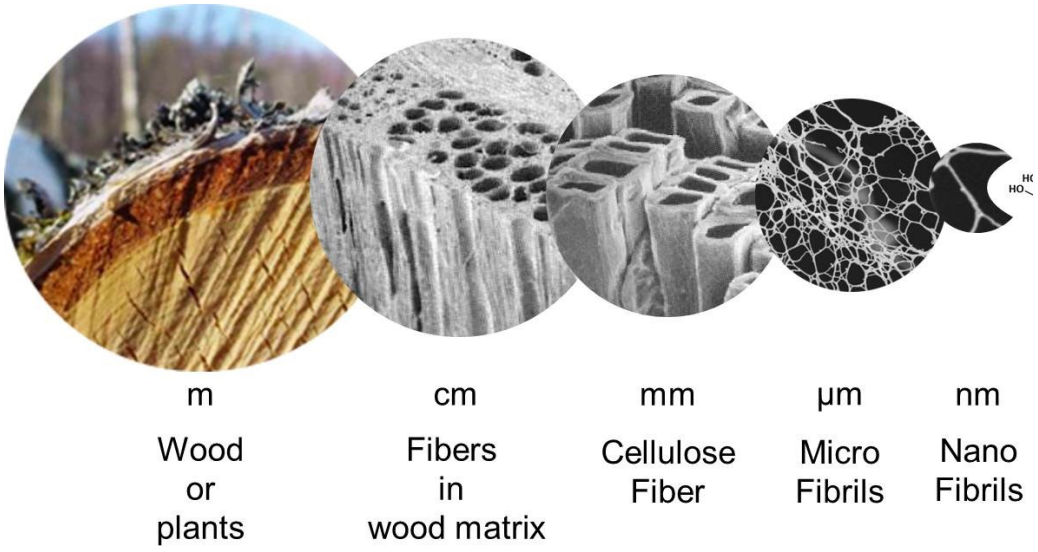

Figure 1. – Extraction of micro and nanofibrils from wood and plants [14].

A problem many countries and municipalities have been struggling against is the increased contamination of streams, rivers, and different bodies of water by heavy metals and oily wastewater. These are produced from various industries, such as food packaging industries, petroleum refineries, vegetable oil and hydrogenated oil manufacturing, and metallurgic industries. This problem has aggravated consistently with the increased industrialization of our world [15]. Oily wastewater pollution has, overtime, become synonymous with nefarious effects on living organisms, marine ecosystems, and general human health. As such, the cleaning of water ecosystems is a relatively simple first step in the development of a symbiotic relationship between humanity and planet Earth [16,17]. With respect to oil-water separation, traditional techniques include oil-water emulsion with air flotation [18], flocculation [19], and oil skimming [20]. While these techniques are well documented, they remain costly and have relatively low efficiency [21]. Alternatives are thus being sought to depollute in an affordable and accessible manner. One of those alternatives being analysed is polyurethane foams [22]. This kind of foam can also be produced using microfibrillated cellulose (MFC). These sustainable and biodegradable foams are very interesting because they can generate a selective absorption process through judicious control of their physical and chemical properties [23].

Due to the sustainability and biodegradability of MFC foams, many processes have been analysed to valorise them on an industrial scale. Wet chemistry has proven its efficiency to some extent in the improvement of the barrier properties of these materials, notably increasing their hydrophobicity. However, these techniques are often incompatible with today's environmental and safety regulations due to the polluting chemicals they require, limiting their potential uses [1,8,11–13]. Plasma treatment, and more specifically, dielectric barrier discharges (DBD) at atmospheric pressure, have been suggested as a "green" way to modify bio-based materials and to bypass wet chemistry disadvantages [14,22,24–28]. The biggest advantage of using such plasmas at atmospheric pressure is that they do not require constant pumping to maintain a chamber at very low pressures, rendering their application on assembly lines easier to implement during continuous, in-line processing [22,29]. In addition, DBDs are characterized by neutral gas temperatures close to room temperature such that they become compatible with heat-sensitive materials such as cellulose-based films and foams [2,30,31]. However, the application of such plasmas to MFC foams is accompanied by a number of scientific and technological challenges. This includes the breakdown physics through these highly complex materials as well as the processing of these microporous and multicomponent structures in presence of reactive species for surface engineering [32–36].

This research project is realized in collaboration with two Canadian companies, namely Plasmionique and FPInnovations. While Plasmionique is interested in the development and optimization of DBD plasma sources for the processing of cellulose-based materials and nanomaterials, the goal of FPInnovations is to valorise and promote Canadian forestry and paper industries through the development of new materials and applications issued from cellulose-based materials and nanomaterials. Very recently, FPInnovations has developed MFC foams in great quantity and is looking at different methods and techniques to valorise them on a competitive, international market. Unfortunately, the valorisation of these foams currently remains complicated. Their high hygroscopicity and hydrophilicity greatly limits their potential applications. We will therefore concentrate our efforts on how the use of DBD plasmas at atmospheric pressure can be used to initiate a physical and/or chemical modification of the MFC

foams to provide a potential solution to the problem brought forth by our industrial partners. Initially, the primary objective will be to analyse and comprehend the breakdown that occurs when plasma discharges are initiated in presence of the MFC foams. Then, these results will be used to synthesise water-repellent layers on and/or in the foams using non-toxic organosilicon precursors. Such studies could then be used as building blocks for an enlarged functionalization potential of DBD sources and MFC foams in today's markets.

From a fundamental point of view, the goal is to characterize the physics driving discharge ignition and sustainment in DBD systems in presence of complex MFC foams. From a technological point of view, the objective is to examine the plasma deposition of functional coatings on these cellulose-based materials to produce sustainable and biodegradable filters that can separate heavy metal particles from wastewater. To adequately introduce the basics of what will be researched and analysed, the following chapter present an overview of the most recent literature on which this project concentrates. Selected research contributions are then exposed in the subsequent chapters in the form of publications recently submitted to major scientific journals in plasma science and technology.

Chapter 2 – General Principles and Literature Review

2.1 - Creation of Non-thermal Plasmas at Atmospheric Pressure

Plasmas at atmospheric pressure offer a unique set of physical and chemical properties. In many cases, however, the relatively high pressure contributes heavily to electron multiplication such that the number densities of charged particles (ions and electrons) can be very high. In addition to electron multiplication involving electron-atom ionization collisions, such plasmas can also generate a lot of heat through electron-atom elastic collisions. For the so-called thermal plasmas, heating is such that the electrons, ions, and neutrals are characterized by comparable temperatures. Such discharge conditions can obviously become very problematic for the treatment of heat-sensitive materials such as wood and wood derivatives (films and foams). For such applications, non-thermal plasmas in which the electron temperature is much higher than those of the ions and neutrals are much more appropriate. One of the most efficient methods for producing non-thermal plasmas with neutral gas temperatures close to room temperature is Dielectric Barrier Discharge (DBD) [1,14,37,38].

2.2 - Dielectric Barrier Discharges

A very simple method of generating a plasma discharge is by applying a potential difference between two electrodes. Over time, it has become common to slow down the electronic avalanche caused by the application of an electric field using a dielectric material and creating what is called a Dielectric Barrier Discharge (DBD) [2]. DBDs imply the presence of, at the very least, one solid dielectric material in the electrode gap. When subject to a direct current (DC), dielectrics will accumulate charge until they “saturate”, upon which they will prevent any electrical current from passing through them. As such, dielectrics are often called insulators. Because of their insulating properties, dielectrics are incredibly useful in plasma physics, as they limit the amount of energy that can be present in the gas gap, rendering an arc transition nearly impossible. However, in order to get any form of discharge at all, the use of an alternating current (AC) is necessary [1,3,10,39–42].

If the amplitude of the applied AC voltage exceeds a certain threshold, the gas breakdown can generate either a spatially-homogeneous discharge or a filamentary discharge allowing for current to flow. The dielectric acting as the anode initially charges itself, acts as a capacitor and, eventually, an insulator by gradually accumulating charges on its surface as the discharge continues (see the workings of a DBD in Figure 2) [43–46]. If only tiny discharge channels, or microdischarges (filaments), were formed initially, more will be generated in different areas as the applied voltage increases to uniformly charge the dielectric. The dielectric eventually saturates in charges and, if the discharge is not stopped beforehand, will act as complete insulator, preventing the discharge from continuing on its own. As the current alternates, what was previously the anode becomes the cathode. Then, charges previously accumulated on the dielectric surface will contribute to a gas breakdown at a lower potential than what was required for the previous discharge [1,10,44]. Hence, the main objectives of a dielectric layer are: (i) to reduce electron multiplication and thus to prevent the formation of highly-destructive arc discharges and (ii) to provide seed electrons from one cycle to the other of the applied AC voltage.

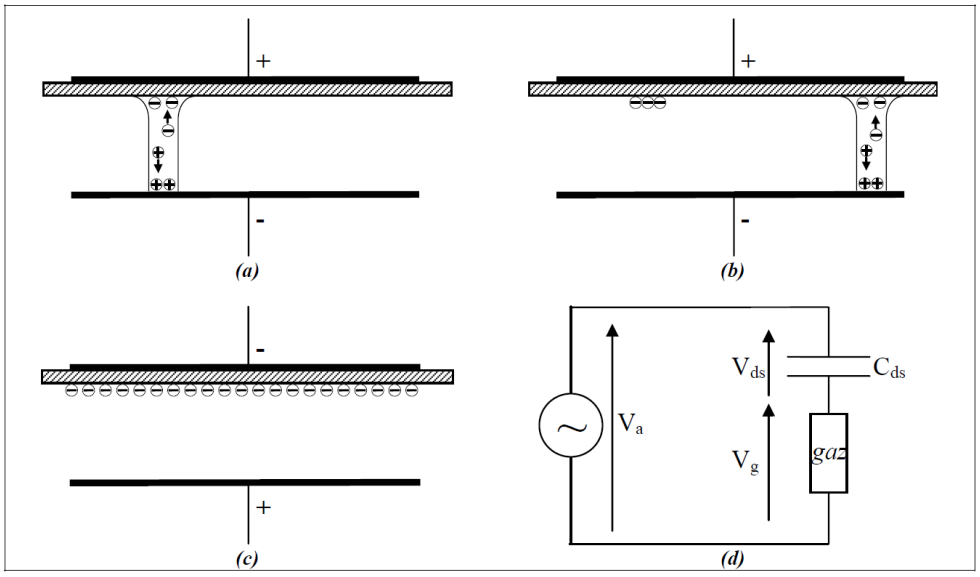

Figure 2. – Principle behind a DBD plasma [1] – (a) Establishment of a first microdischarge – (b) Attenuation of the first micro-discharge and beginning of a new one in a different position – (c) Polarity applied to system alternates – (d) Electrical schematic of the discharge [43]

2.3 - Breakdown and Discharge Regimes

There exist two possible breakdown regimes in a plasma discharge. The first is called a Townsend breakdown whereas the second is called a streamer breakdown [10,46,47]. Each will happen depending on the experimental conditions. A discharge will be heavily dependent on the pressure and the gas gap. Normally, a streamer breakdown will be a direct result of a higher pressure-distance product. In atmospheric pressure DBDs, the gas gap is generally shorter than a few millimetres, and the pressure is, of course, fixed at one atmosphere. As such, it is often very hard to alter the pressure-distance product. If left to itself, breakdowns at atmospheric pressure will therefore tend towards streamer breakdowns. This will lead to multiple highly energetic filaments randomly distributed in time and space in the gas gap. These filaments can be very destructive when a material is processed, because the filaments locally exhibit a significant amount of heat [48,49]. An example of each possible breakdown regime in a DBD at atmospheric pressure is shown in Figure 3.

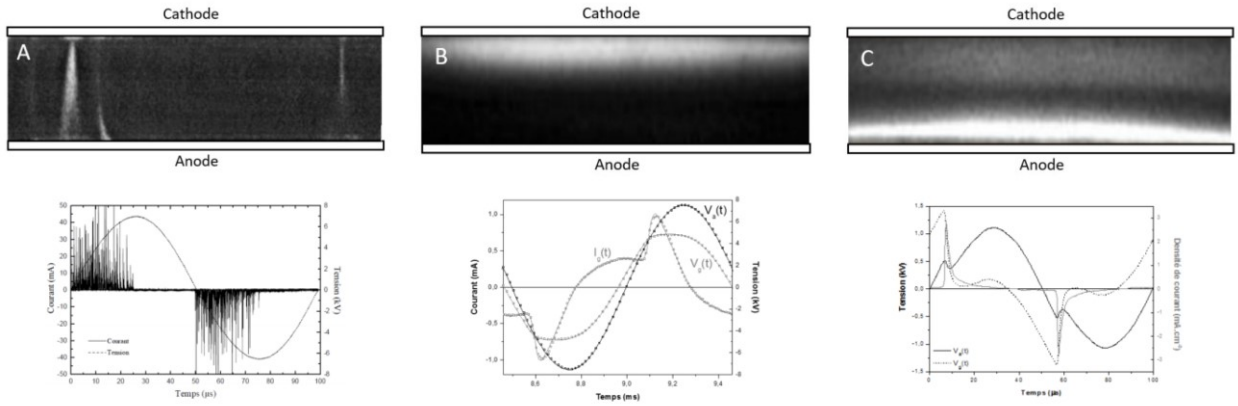

Figure 3. – Characteristics of possible breakdown regimes in a DBD at atmospheric pressure. Gate width: 10 ns for (A), and 100 ns for (B) and (C) [1].

The natural outcome of the streamer breakdown is the filamentary discharge. This produces a multitude of micro-discharges which generate sporadic current readings in current-voltage characteristics [3]. An optical image of a filamentary discharge and its corresponding electrical signature is shown in figure 3A. As can be seen, this regime produces luminous filamentary channels randomly distributed in time and space [3].

Townsend breakdown is associated to a much slower ionisation process producing fewer ionised species than it would in a streamer breakdown (see Table 1). Altering the ionization kinetics will thus prioritise one regime over another. In order to slow said ionisation, a secondary species is typically added to the nominally pure plasma gas. This admixture is usually selected such that its ionization energy is comparable or lower than a metastable state of the main plasma gas. For example, in helium with a nitrogen admixture, the helium metastable state is first created by electron-impact excitation on ground state helium atoms. Due to the presence of N_2, ionisation can occur through energy exchange reactions between helium metastable atoms and ground state nitrogen molecules. These so-called Penning ionization reactions reduce the probability for direct electron-impact ionization of helium atoms, thus slowing down the ionization process by prioritising a Townsend rather than streamer breakdown [4,10,41,45].

Townsend breakdown is analyzed by the voltage-current characteristics displayed in Figure 4. Initially, increasing the voltage directly increases the current by electron-atom ionization collisions. As voltage increases up to values higher than the breakdown voltage (identified as V_B in Figure 4), ionisation processes will increase the number of electrons in the system very rapidly, meaning the current will increase substantially. This is the phase where current is said to be self-sustained. Depending on the experimental conditions, intermittent discharges can drag along the transition region and can ultimately lead to a normal glow discharge [4,10].

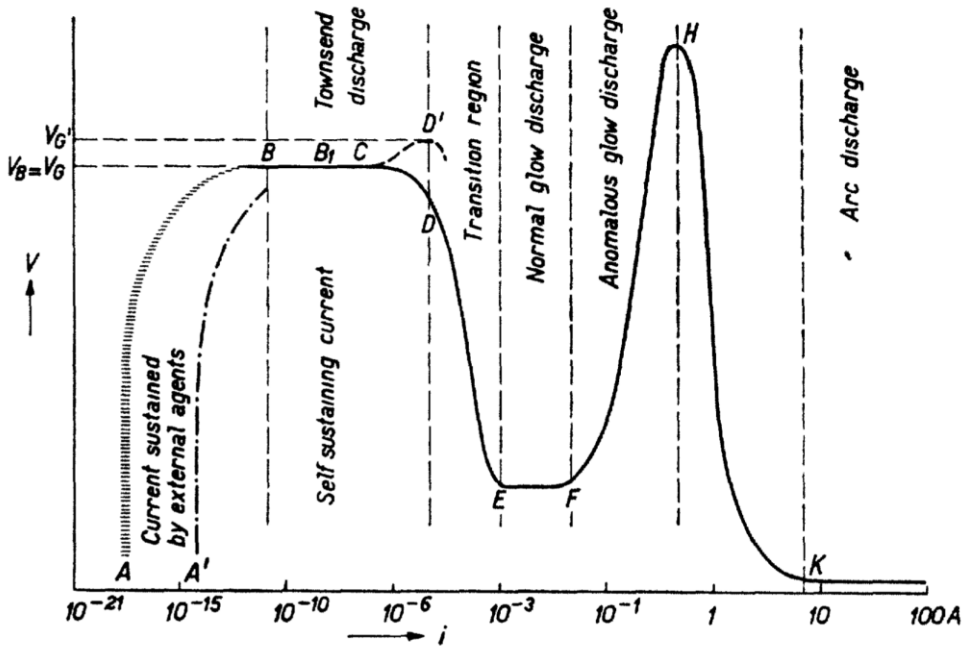

Figure 4. – Current-voltage (V-I) characteristics in a Townsend breakdown [50]

There are two discharge regimes that can occur in a Townsend breakdown. The first is called Atmospheric Pressure Townsend Discharge (APTD, corresponds to figure 3B), or simply a Townsend discharge, and the second is named Atmospheric Pressure Glow Discharge (APGD, corresponds to figure 3C), or simply a glow discharge. Townsend discharges typically occur in gas mixtures that contain nitrogen gas. Glow discharges are reliant on Penning effect and typically occur in rare gases with an admixture (for example, He with N_2 and Ar with NH_3) [3,43,51]. From an electrical standpoint, these two different forms of homogeneous discharges imply a single current peak per half period of the applied voltage. Glow and Townsend discharges are very hard to differentiate by the naked eye. However, they can be distinguished by optical imaging. While Townsend discharges generate light for about the entirety of the half period of the applied voltage (with a more important signal close to the anode, Figure 3B), glow discharges concentrate their light emission on a very brief but strong light signal (with a more important signal close to the cathode, Figure 3C). Some fundamental values of the different discharge regimes are summarized in Table 1 [1,52].

	Filamentary Discharge	Glow Discharge	Townsend Discharge
Time	1-100 ns	1-5 µs	Half period
Maximum Current Density [$mA.cm^2$]	10^3-10^4	1-10	0.1-5
Maximum Electronic Density [m^{-3}]	10^{14}-10^{15}	10^{16}-10^{17}	10^{13}-10^{14}
Maximum Ionic Density [m^{-3}]	10^{20}	10^{17}	10^{17}
Maximum Metastable Density [m^{-3}]	10^{19}	10^{17}	10^{19}
Maximum Power Density [$W.cm^{-2}$]	10	1	5

Tableau 1. – Typical values characterizing the various discharge regimes in a DBD configuration at atmospheric pressure [22]

As shown in Table 1, a filamentary discharge has power density significantly more pronounced than any other type of homogeneous discharges [29,53,54]. In addition, this power is highly localized in time and space. Filamentary discharges can obviously have a strong impact on the integrity of plasma-exposed materials; an example is shown in Figure 5 [23,49,50,55].

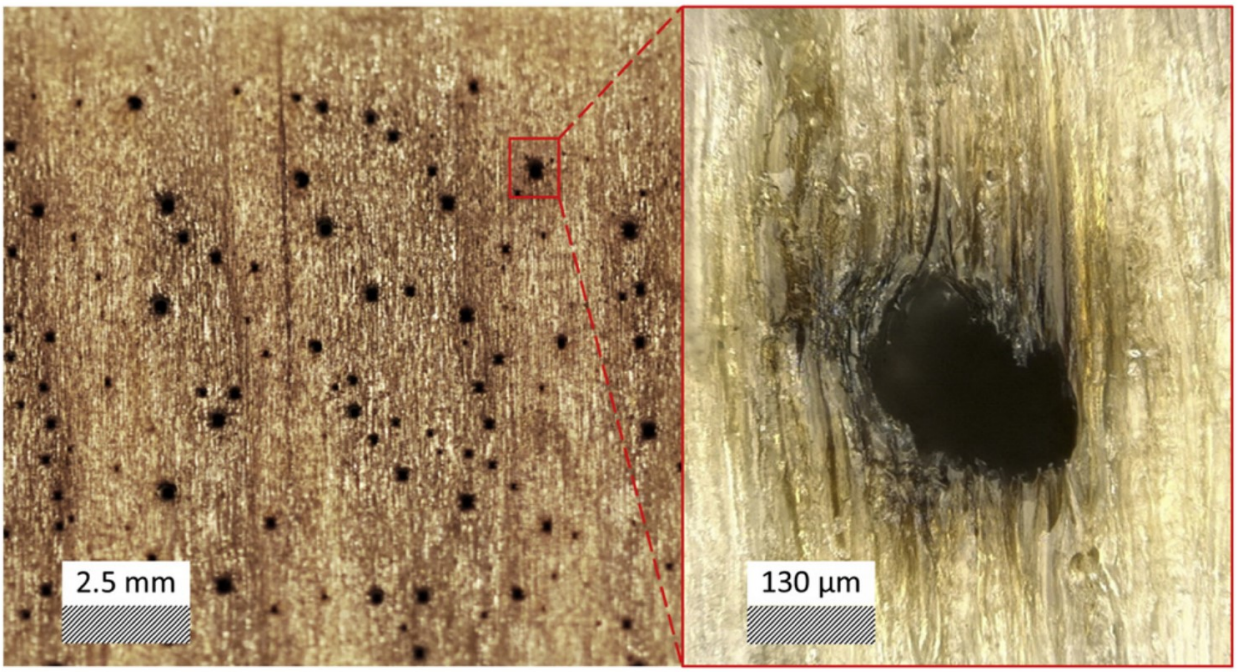

Figure 5. – (Left) Optical image of the wood substrate treated with a N_2 filamentary discharge. (Right) Zoom of a burn on the wood substrate [55]

As shown in Figure 5, filamentary discharges can generate significant damage on heat-sensitive materials. In the specific case of wooden substrates, the authors have observed a significant amount of burn marks on the surface of wood samples that had been subjected to a filamentary discharge. Moreover, the random distribution of the burn marks had burn diameters varying between 10 µm and 100 µm, which is similar to the size of the footprints of microdischarges. These kinds of damages were not present in a glow discharge on wood, in part due to the significantly reduced power densities and the much more uniform discharge configuration that is typical of these discharge regimes [55,56].

2.4 - Dielectric Barrier Discharges in Presence of Complex Materials

Discharges occurring in presence of complex materials such as microporous and multicomponent materials is a relatively new branch of plasma science and technology. As such, very little is understood regarding the plasma discharge processes and properties in presence of these materials. It remains, to this day, an expanding field of research. One of the complex materials analysed in detail in presence of DBD at atmospheric pressure is wood. Research of

discharge conditions and regimes in the presence of wood is sparse, but high-quality. Wood is a good reference for the research on microfibrillated cellulose (MFC) foams since it is also issued from woody biomass and has cellulose as its main constituent. Unfortunately, scientific papers on plasma processing of MFC foams do not exist, and though some research teams have explored the processing of different types of materials through different techniques [57–60], none have delved in the realm of the underneath plasma science. Recent literature in the plasma processing of a wood substrate has demonstrated some very important effects and phenomena to consider when producing plasma discharges in contact with cellulosic materials; some of these aspects are described below [23,34,55,56,61].

2.4.1 - Substrate Outgassing

Outgassing is the process of removing gases adsorbed on the surface of a material. This aspect is particularly important for porous materials characterized by high-surface-to-volume ratios [32]. Typically, materials outgassing is done by heating in vacuum. However, in the case of cellulose-based materials such as wood or MFC foams, heating is not an option since thermally-activated physical and chemical modification can occur [55]. Other techniques must therefore be developed and used if substrate outgassing is required.

Figure 6 presents the evolution of the optical emission spectrum of a nominally pure He DBD operated in a glow discharge regime with a bulk wood samples placed on the bottom electrode. While the optical signature of He DBDs is typically dominated by He atomic lines between 600 and 800 nm, significant emission from N_2 bands (300-500 nm) and O atomic lines (777 nm) can also be seen in Figure 6 [32,49]. These features arise due to substrate outgassing, the release of air trapped in the wood microstructure. It is further shown that, over the range of experimental conditions investigated by the authors, plasma-activated wood outgassing takes up to sixty minutes to vanish [32,49,55].

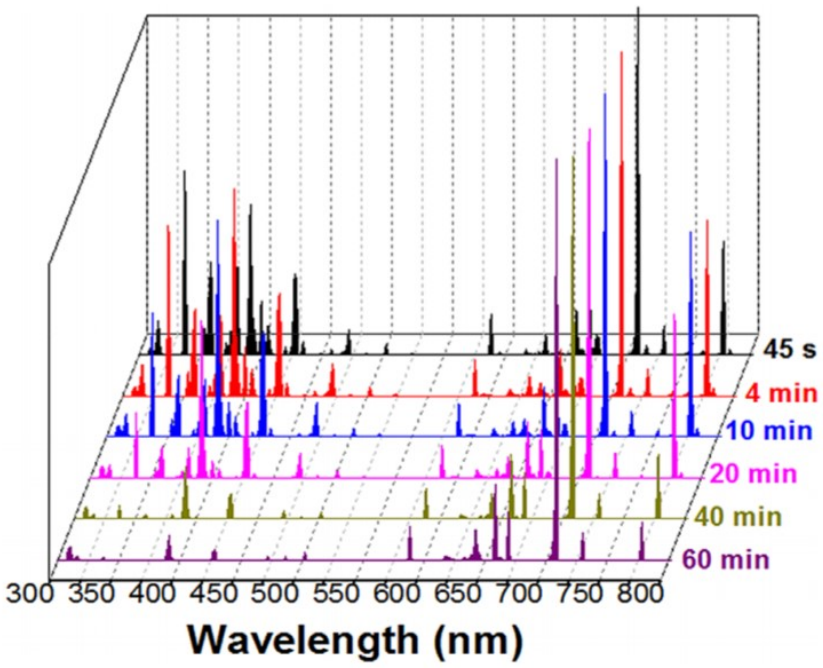

Figure 6. – Optical emission spectra of He DBD in presence of a wood substrate. All spectra recorded as a function of plasma treatment time reveal the presence of N_2, N_2^+, and O due to substrate outgassing [32]

The release of N_2 and O_2 from the sample in the high-purity He DBD obviously has a strong effect on the discharge physics. From the optical emission spectroscopy measurements reported in Figure 6, coupled with collisional-radiative modeling, Levasseur et al. have shown that the electron temperature decreases, and the population of metastable helium atoms increases during substrate outgassing. This can be seen in Figure 7. Over the range of experimental conditions investigated by the authors, the density of metastable helium atoms increases by about two orders of magnitude between 0 and 60 minutes of substrate outgassing. Such variation is consistent with a very strong quenching of helium metastable species by collisions with nitrogen and oxygen molecules [10,32,41]. However, if the substrate in placed in vacuum for several hours before plasma treatment, Figure 7 reveals comparable discharge properties immediately after discharge ignition rather than after an hour for the non-outgassed samples. This clearly champions the potential importance of outgassing a porous cellulosic substrate prior to treatment in a DBD at atmospheric pressure [32]. The effect of outgassing during plasma processing of MFC foams will be explored later in this work.

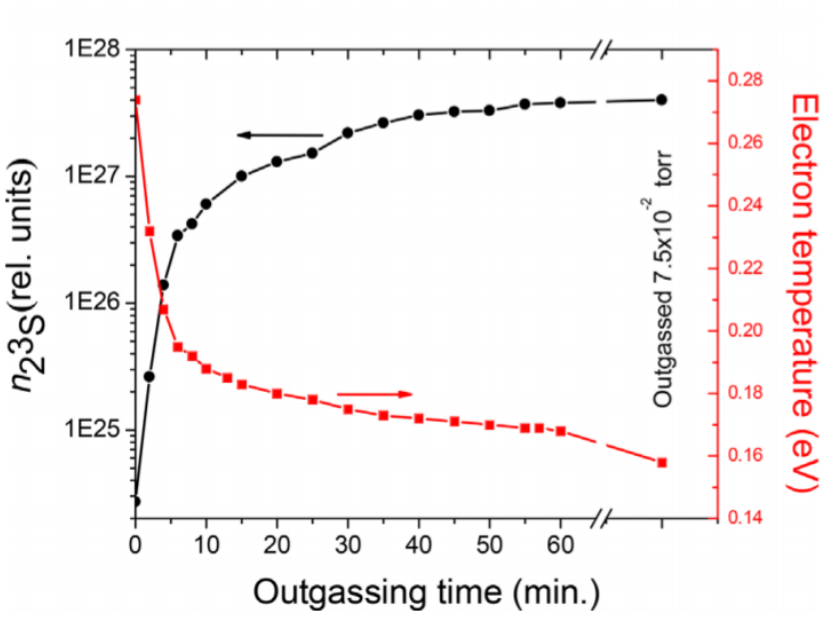

Figure 7. – Influence of substrate outgassing time on selected properties of He DBD in presence of a wood substrate. The red line indicates electronic temperature and the black line indicates the population of metastable He atoms (relative units) [32].

2.4.2 - Discharge Localisation Phenomenon

Because of their complex microstructure, cellulosic materials exposed to atmospheric-pressure plasmas can also induce spatial inhomogeneities in the physical and chemical properties of DBDs. As an example. Levasseur et al. have reported electrical and optical measurements of helium DBDs at in the presence of fully-outgassed wood substrates. As presented in Figure 8, the discharge show more intense light emission intensities on early (less dense) versus late wood (more dense) sections of the strongly inhomogeneous wood substrate. Multiple analyses were made, beginning by the variations of the peak-to-peak voltage, the frequency, gas gap, etc., but the peculiar spatial distributions in the light emission patterns were still observable. Moreover, current-voltage characteristics were still very consistent with a glow discharge regime [2,10,45]. That is, they were characterised by a single and periodic discharge for every half-cycle of the applied voltage, without any apparent variations from the light and dark regions. Further analyses

were thus made using optical emission spectroscopy, with measurements taken on the emitting regions and in the dark regions to gain an idea of the electron temperature across the whole wood substrate surface (see Figure 9).

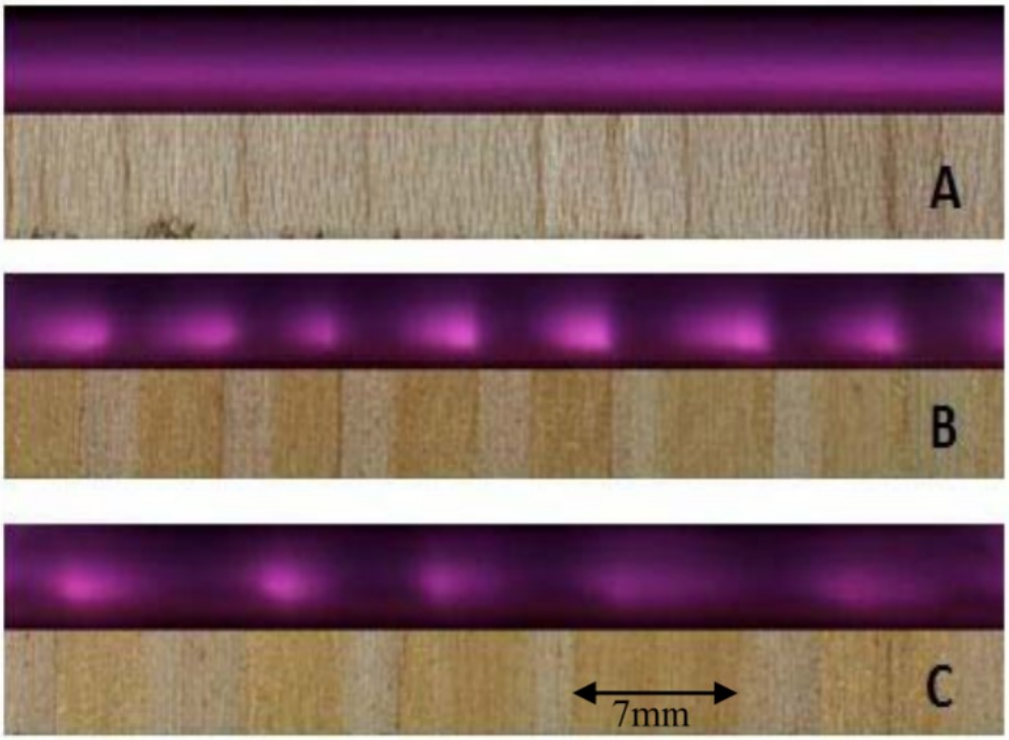

Figure 8. – Spatial distribution of the helium plasma emission in presence of a (A) sugar maple, (B) Douglas pine with tight and (C) wide late and early wood sections [33]

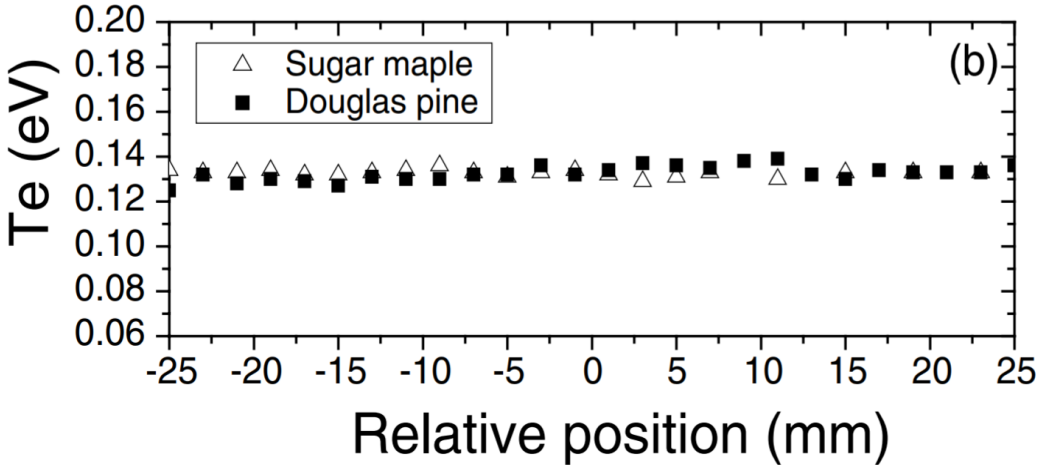

Figure 9. – Evolution of the time-averaged electron temperature for the sugar maple and Douglas pine samples [33]

As shown in Figure 9, the electron temperature remained constant, maintaining relatively identical values for both the light and dark discharge zones. Moreover, the 0.13 eV global average electron temperature is comparable to the ones typically reported for He DBDs in a homogeneous regime [32–34]. The team pushed their analysis further through an ingenious method of charging the wood samples and measured the potential decay as a function of time. There, they found that overall decay time of late wood was much slower than early wood. Because the characteristic time constant is inversely proportional to the square root of the product of capacitance and resistivity, the observed discharge localization could a priori be linked to either changes of the dielectric constant or resistivity across the wood sample. It was then confirmed through simulations that only a modulation of the dielectric constant on early (low capacitance) versus late (high capacitance) wood can explain the amplitude of the changes in the discharge localization phenomena through spatial changes of the voltage applied locally to the gas [33]. Such analysis will be used as building blocks to understand discharge ignition and light emission patterns in plasmas sustained in presence of MFC foams.

2.4.3 - Transport Phenomenon

The phenomenon referred to as transport is of crucial importance during processing of porous materials such as wood and wood derivatives. In such systems, plasma-surface interactions are not limited to the topmost surface but rather to the whole substrate volume due to its high surface-to-volume ratio [62]. Transport phenomena were found to be particularly important in the context of textile treatments by plasma discharges. For example, Morent et al. [38,63] have analysed plasma penetration in textiles by stacking multiple layers over one another and individually analysing each. To do so, they used a DBD configuration at a pressure of 1 kPa. They discovered that a homogeneous discharge regime in a DBD configuration increased the transport of reactive species through the treated material's volume, and that a reduction in filaments derived from a filamentary discharge contributed to a more efficient treatment [38,63].

The pressure at which a discharge occurs was also found to have an important impact on the transport processes. Poll et al. [64] have analysed plasma-surface interactions in porous materials, this time in a plasma jet configuration. They, like Morent et al., had stacked textile layers one over the other to obtain a qualitative idea of the transport processes that occurred. They have found that low-pressure discharge conditions were optimal to obtain appropriate and thorough incorporation of plasma-generated species. They also attempted this experiment in atmospheric-pressure plasmas, and found that negligible amounts of incorporation had occurred [38,55,63,64]. On the other hand, Wang et al. [65] have demonstrated, in opposite fashion to Poll et al., that it is possible to obtain adequate incorporation of reactive species in a textile at atmospheric pressure in a plasma jet configuration. They found that larger pore sizes lead to deeper penetration of the plasma in the material, and that the absorption of reactive species is therefore influenced significantly by pore size and structure [62,65,66].

For diffusive transport of reactive species to be efficient, the mean free path of these reactive species must be close, or greater, than the mean size of the pores on the substrate [46,67]. Otherwise, there is substantial losses of these species, and diffusive transport

through the substrate's volume is low. As such, many of today's existing literature has focused their effort on low pressure DBD configurations to ensure that the mean free path of the reactive species remains high. This is, in part, because today's analyses and measurements are done on textiles, which are not very porous [38,63]. Unfortunately, despite a thorough analysis of today's scientific literature, few quantitative information was found on the physics reigning diffusive transport. Most of what exists today remains very qualitative, however, the information garnered from such publications do give a very good idea of what to expect regarding diffusive transport and direct penetration in materials with controlled porosity. Therefore, despite the confirmation by multiple references [38,62,63,65,66,68] that indicate that very little transport can be observed at atmospheric pressure in a DBD configuration, the high porosity of the MFC foams analysed in this work bring forth a unique perspective on a problem that has rarely deviated from a certain norm, indicating a high possibility of interesting and unique observations. Indeed, analysis through cellulosic films of similar properties to the MFC foams studied in this work have demonstrated very promising results [69].

2.5 - Dielectric Barrier Discharges for Thin Film Deposition

Thin film coatings using DBDs operated in reactive gas mixtures are a field of plasma science and technology presently exploding in interest worldwide as a sustainable, eco-friendly, low-cost, and simple way of altering physical and chemical interactions between substrates and their environment. This interest stems from the desire to valorise and utilise unique, sustainable, and widespread products in a vast array of new ways. Often however, these products are limited by their physical and/or chemical nature, and greatly limits their potential. Wet chemistry procedures exist. However they, at times, do not respect the ever-increasing environmental norms of our day [50,70]. Many industries and labs have thus turned to plasma processes to confer these thin film coatings. One recent example is the plasma deposition of water-repellent coatings on glass, plastic, and wooden samples [23,55,71–74].

The adequate and precise deposition process of thin film coatings on substrates remains a very complex phenomenon. Thin films can be produced by adding a precursor to a plasma discharge which has the chemical components scientists seek to confer to substrates. For instance, the use of non-toxic hexamethyldisiloxane (HMDSO) allows the deposition of a non-polar layer on the surface of certain materials, which, in turn, allows for these materials to acquire a certain hydrophobicity [50,55,71]. An example is shown in Figure 10 for wood samples exposed to either He or He/HMDSO plasmas. Analysis of the surface wettability through water contact angle (WCA) measurements indicated that freshly sanded wood samples treated in He/HMDSO plasmas became more hydrophobic with WCAs in the 120–140 degree range depending on treatment time. Attenuated Total Reflectance Fourier Transform Infrared (ATR-FTIR) spectroscopy measurements on samples exposed to He/HMDSO plasmas revealed the deposition of hydrophobic organosilicon groups. In presence of oxygen species in the gas phase, carbon-containing groups can be removed, leading to the plasma deposition of silica-like layers [50,51,55].

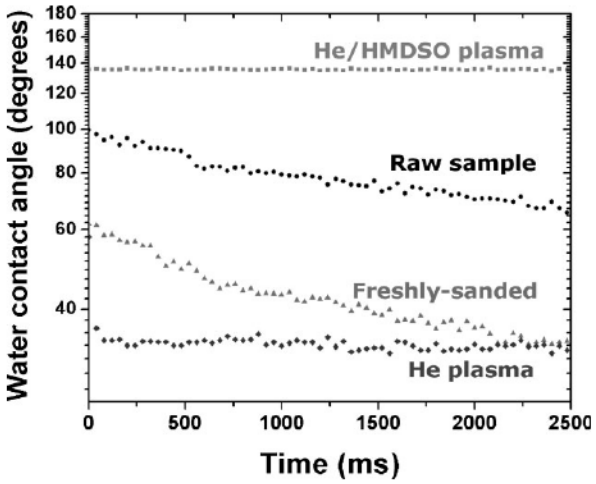

Figure 10. – Dynamics of the wetting process on sugar maple wood samples exposed to He and He/HMDSO (100 ppm) plasmas. Water contact angles from raw and freshly sanded sugar maple samples are also shown for comparison [50]

Massines et al. have analysed the physics driving homogeneous DBDs in presence of HMDSO and N_2O, including information on deposition efficacy of SiO_x thin films [51]. From current-voltage characteristics, the authors found that the discharge remained homogeneous for modest injection levels of HMDSO and N_2O. In the plane-to-plane DBD configuration examined, all gaseous species enter from one end of the gas gap and flows over the top of the substrate that is being plasma-treated. In such conditions, one would think that deposits of thin films would be non-uniform across the whole substrate surface. However, through judicious choice of the operating conditions [67], a relatively homogeneous SiO_x coating is achieved over the entire substrate surface, which has also been confirmed by additional references [46,49,50,55,75]. Some measurements have also been done in a DBD operated in a filamentary discharge regime [51]. This strongly affects the uniformity of the coating, as the discharge is localised in specific areas, and not over the entire surface.

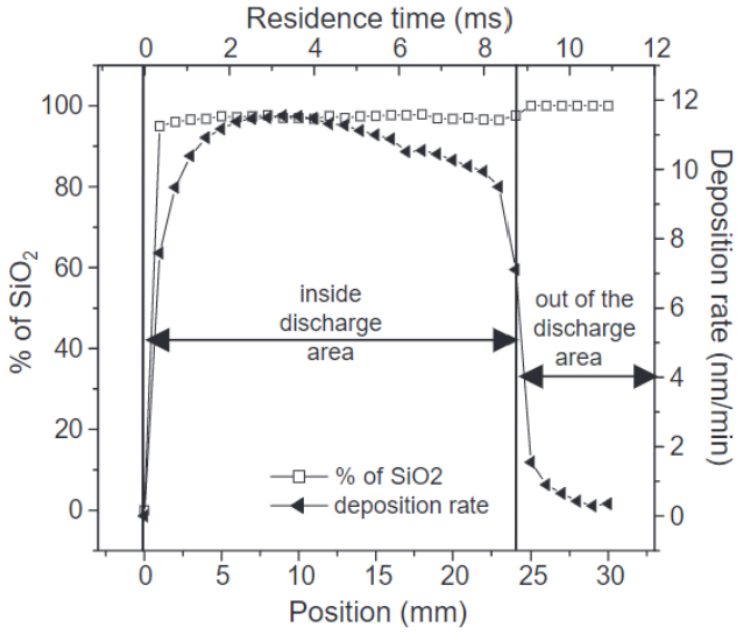

Figure 11. – Thin film coating percentage effiency as a function of position on the substrate along the gas flow lines in plane-to-plane DBD [51]

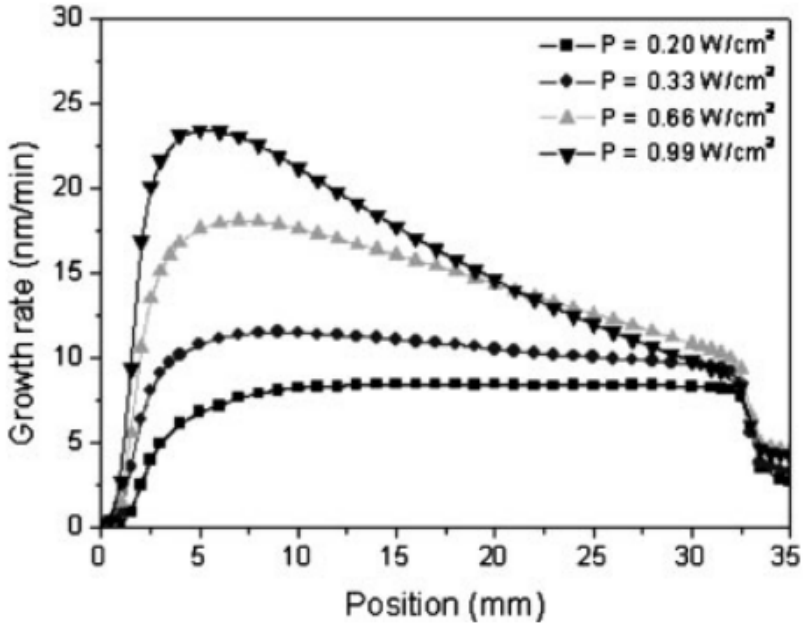

Figure 12. – HMDSO growth rate profile over time along the gas flow on a surface through different power values [67]

While the homogeneity of plasma-deposited coatings can readily be controlled through judicious control of the operating conditions (for example, the discharge power as shown in Figure 12), the porous microstructure can also play an important role. In such cases, plasma deposition is not limited to the topmost surface but also occurs in the substrate volume. This aspect was recently explored by Profili et al. [14] and Babei et al. [69] for organosilicon coatings deposited on films formed of cellulose materials. In such cases, films with different thicknesses and chemical composition can be obtained along the gas flow lines [69]. These effects, however, vanish for films with lower porosities due to the corresponding decrease of diffusive transport phenomena.

2.6 – Summary

In this chapter, the physics driving homogeneous and filamentary DBDs at atmospheric pressure was summarized. When applied to the processing of complex substrates such as cellulose-based materials and nanomaterials, a number of interesting additional phenomena

arise, including substrate outgassing, discharge localization, and transport of plasma-generated species in the volume. These aspects obviously become even more complex during thin film deposition, for example for the formation of water-repellent surfaces. In the following chapters, this literature review will be used to examine the modification of MFC foams derived from woody biomass in DBDs at atmospheric pressure.

Chapter 3 – Results and Analysis

3.1 - Introduction

As underlined in the previous chapter, discharges in the presence of complex, porous, foams issued from wood biomass is a relatively new field of research, with little to no scientific publication on the subject. Yet, some qualitative analysis done with open-cell polyurethane foams have demonstrated incredibly interesting potential properties of plasma processes. Indeed, Armenise et al. and Fanelli et al. have shown that plasma-treated polyurethane foams can be used in the decontamination of water by having selective absorption of heavy metals [73,76]. In other fashion, a renewed interest in the potential valorisation of cellulose, a tremendously easy to generate substance, and a very green material, has allowed for the synthesis of MFC foams.

This chapter is first dedicated to the presentation of different discharge phenomena that occur in DBDs at atmospheric pressure where MFC foams taking up the entire gas gap volume are used. The results are presented as a publication entitled "**Characterization of non-thermal dielectric barrier discharges at atmospheric pressure in presence of microfibrillated cellulosic foams**" by Louis-Félix Meunier, Jacopo Profili, Sara Babaei, Siavash Asadollahi, Andranik Sarkissian, Annie Dorris, Stephanie Beck, Nicolas Naudé, and Luc Stafford, recently submitted to Plasma Sources Science and Technology (manuscript #PSST-103959). Further on, an analysis on functional coatings that can be deposited on MFC foams for effective separation of oily wastewater is described. The results are presented as a publication entitled "**Modification of Microfibrillated Cellulosic Foams in a Dielectric Barrier Discharge at Atmospheric Pressure**" by Louis-Félix Meunier, Jacopo Profili, Sara Babaei, Siavash Asadollahi, A. Sarkissian, Annie Dorris, Stephanie Beck, Nicolas Naudé, and Luc Stafford, recently accepted for publication (after minor revision) in Plasma Processes and Polymers (manuscript #PPP-103959). For both studies, Louis-Félix Meunier contributed to all data acquisition, analysis, and wrote the first draft of the manuscripts.

3.2 - Characterization of non-thermal dielectric barrier discharges at atmospheric pressure in presence of microfibrillated cellulosic foams

Louis-Félix Meunier[1,2], Jacopo Profili[1], Sara Babaei[1], Siavash Asadollahi[3], Andranik Sarkissian[3], Annie Dorris,[4] Stephanie Beck,[4] Nicolas Naudé[21], and Luc Stafford[12]

[1]*Département de physique, Université de Montréal, Montréal, Québec, H2V 0B3, Canada*

[2]*LAPLACE, Université de Toulouse, CNRS, INPT, UPS, Toulouse, France*

[3]*Plasmionique Inc., Varennes, Québec, J3X 1S2 Canada*

[4]*FPInnovations, Pointe-Claire, Québec, H9R 3J9, Canada*

ABSTRACT

Plasma processing of sustainable polymers from renewable resources has recently gained significant interest. This work reports the ignition of plane-to-plane dielectric barrier discharges at atmospheric pressure operated in nominally high-purity helium with microfibrillated cellulose (MFC) foams derived from woody biomass taking up the entirety of the gas gap. Over the whole range of experimental conditions examined, discharge ignition and propagation mostly occurs through the foam from one electrode to the other (volume discharge). For fully-outgassed foams, current-voltage characteristics and optical imaging revealed a glow-like discharge regime at 60 kHz and a filamentary behaviour at 10 kHz. However, significantly less plasma-induced damage was observed through the MFC foams at 10 kHz. For non-outgassed samples exposed to the helium gas flow, gaseous species trapped in the MFC foams yielded to a significant increase of the discharge power and thus caused more significant damage to the cellulosic material.

KEYWORDS: Cellulosic materials, plasma-cellulose interactions, dielectric barrier discharges, optical and electrical diagnostics.

[1] Electronic mail: Nicolas.Naude@laplace.univ-tlse.fr
[2] Electronic mail: Luc.Stafford@umontreal.ca

3.2.1 - Introduction

Today, governments worldwide are gradually implementing severe penalties and sanctions on polluting industrial processes. As a result, many companies have incentive to seek out alternative processes and materials that will allow them to reduce their carbon footprint. For this reason, bio-based materials, as well as processes to modify them, have been thoroughly studied in the literature. In this context, cellulose-based products have been highlighted as a promising alternative to oil-sourced products [5,6]. Cellulose is an organic material offering incredibly interesting properties and constitutes between 35% and 50% of all planetwide plant-based biomass, making it widespread and accessible in large quantities [5–9]. Recently, new barriers having improved properties for the packaging industry have been developed using chemically modified cellulose. Unfortunately, most modification methods such as extrusion coating and surface sizing [8,11–13] do not meet environmental standard requirements. In particular, repulping issues are a serious problem in packaging applications, as most hydrophobic liners are non-repulpable, which prevents recycling of packaging products.

Non-thermal plasma processes have been suggested as a “green” way to modify bio-based materials and to bypass wet chemistry disadvantages [24–28,71]. Among the different non-thermal plasma sources, plane-to-plane dielectric barrier discharges (DBDs) at atmospheric pressure, which provide low ionization degrees and low neutral gas temperatures, represent interesting building blocks for the treatment of heat-sensitive materials [2,30,31]. DBDs are characterized by at least one dielectric placed between the electrodes. The dielectrics are responsible for limiting the amount of energy that can transit through a discharge canal, thus preventing arc transition. These systems are easily implemented in industrial assembly lines because they do not require expensive vacuum equipment [54]. The physics driving these plasmas have been studied in depth [10,40–42,44,77]. Despite the fact that the functionalization and/or modification of cellulose-based materials and nanomaterials by DBDs has become a “hot topic” in the scientific community [35,36,50,61,73,78–81], the spatial and temporal phenomena driving plasma-cellulose interactions remain in many cases poorly understood [35,36]. Levasseur

et al. have characterized the effect of different wood substrates placed on the bottom electrode on the fundamental properties of plane-to-plane DBDs (*i.e.* discharge regime, electron density, electron temperature, etc.) [32,34,82]. Very little research has been done on the interaction of DBDs with more complex materials such as micro-porous foams. Morent *et al.* have presented the different ways to functionalize porous textiles through non-thermal plasma treatments. In particular, they have highlighted the numerous challenges linked to the treatment of polypropylene films with nitrogen DBDs [83]. Fanelli *et al.* have studied thin film deposition on open-cell polyurethane foams in a helium DBD at atmospheric pressure to modify their surface energy [73,78].

This work is focused on the analysis and overall comprehension of the interaction between DBDs at atmospheric pressure and microporous foams made of microfibrillated cellulose (MFC). Electrical and optical diagnostics have been used to measure different aspects of the discharge ignition and propagation, in line with the formation of plasma-induced damage. Experiments are carried out in helium because of its low breakdown voltage, the relative ease to obtain the glow-discharge regime and the presence of high-energy metastable atoms (19.8 and 20.6 eV above ground state) that not only participate in the discharge kinetics through Penning ionization, but are also very efficient to excite impurities present in the discharge gap [77].

3.2.2 - Experimental details and data analysis methods

3.2.2.1 - Experimental setup

The experimental setup consisted of a vacuum chamber in which a plane-to-plane DBD cell was installed. Two electrodes (38 mm × 38 mm in size) were made using silver conductive paste. The electrodes were painted on alumina plates (dielectrics). Glass shims were placed along the sides of the alumina plates to align and direct the gas flow in a 3-mm gas gap. A modified experimental setup was also used for additional optical analyses. In this case, the top dielectric and electrode were made with indium tin oxide (ITO) conductive material on a glass dielectric.

Due to the different configuration, the electrodes were smaller (30 mm × 38 mm); every other parameter was identical. This configuration allowed an intensified charged-coupled device (ICCD) camera to be installed over the top of the experimental setup to record spatially- and temporally-resolved discharge emission. Prior to each experiment, a vacuum with a base pressure of about $5x10^{-3}$ mbar was maintained in the chamber of both systems.

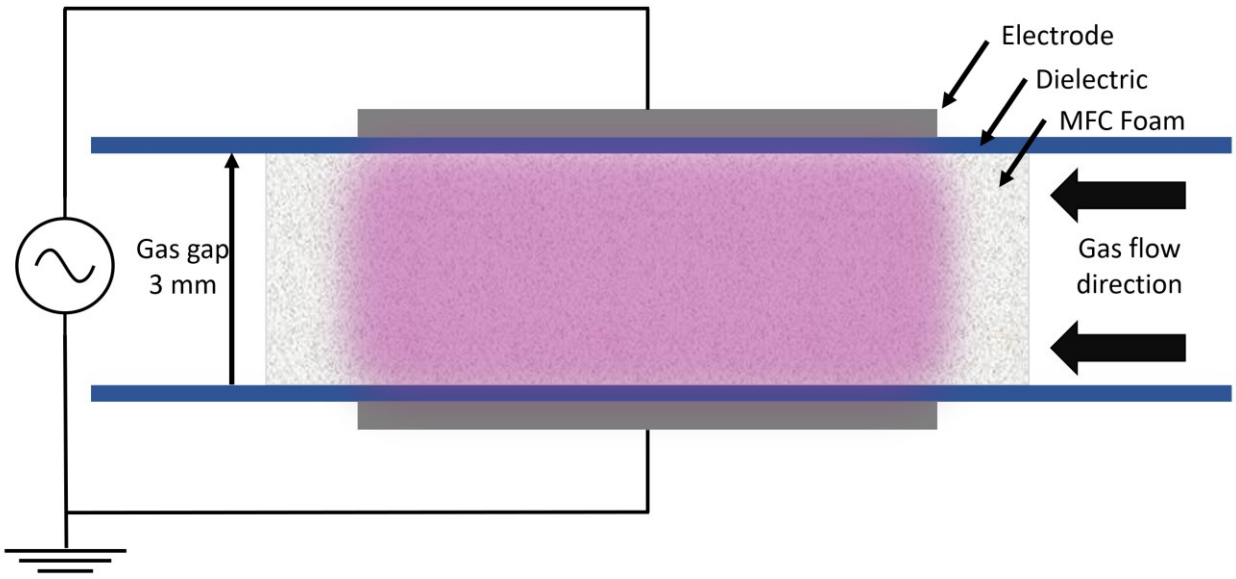

Figure 13. – Schematic of the apparatus used for the production of DBDs in nominally high-purity pure helium with microfibrillated cellulosic (MFC) foams taking up the entirety of the gas gap.

MFC foams were prepared and provided by FPInnovations. Briefly, a suspension of cellulose microfibrils at 0.3wt% was lyophilized in a REVO85 freeze dryer from Millrock Technology. This specific concentration is important because it directly affects the density and porosity of the MFC material before plasma treatment. It must be noted that the 5 mm-thick MFC foams used in this work were very fragile. Prior to the DBD treatment, the untreated foams were delicately placed into the gas gap of the DBD. The foams were cut in compact 40 mm × 70 mm rectangles and placed on the lower dielectric. To avoid any edge effect during the DBD treatment, the entire electrode surface was covered with the cellulosic material. The latter was secured on

the dielectric using Kapton tape placed at both extremities. This allowed the MFC foams to be effectively squeezed between both dielectrics, ensuring proper contact with both elements. In addition, in this configuration the foams occupied the entirety of the gas gap volume. Because of the complex physical conditions, each sample subjected to a discharge was significantly modified, and was not re-used for additional measurements.

DBD was sustained in gas flows of nominally high-purity He (Alphagas 1 - 99.999% purity). To maintain atmospheric-pressure conditions, the chamber was slightly pumped while the gas was constantly injected at one end of the discharge gap with a flow of 4 standard litres per minute (SLM). For DBD ignition, a sinusoidal electrical voltage was applied between the two electrodes using a waveform generator (Keysight 33210A Function/Arbitrary Waveform Generator) coupled to a linear power amplifier (Crest Audio CA18). A protection resistor of 4 Ω was inserted at the amplifier output in series with the primary of a Montoux step-up transformer (600 VA, 60 V/9 kV). The discharge cell was connected to the transformer's secondary in series with a 50 Ω resistor or a 220 nF capacitor in order to measure the current or the charge, respectively. All signals (current I, charge Q, and voltage V) were monitored using an oscilloscope (Teledyne Lecroy Wavesurfer 3024). In this work, the amplitude of the applied voltage measured using a high-voltage probe (P6015A, 75 MHz, 1000:1 from Tektronix) was set at 3 kVpp. Two frequencies, either 10 kHz or 60 kHz, were used in order to probe the effects of low (~0.5-1.5 W) and high power (~5-15 W) on the MFC foam.

3.2.2.2 - Characterization methods

In addition to current-voltage and charge-voltage characteristics, images of the discharge were captured using an ICCD camera (Princeton Instruments PI-Max 3) with a spatial resolution of 150 µm/pixel. Unless otherwise mentioned, the camera integrated light on a complete half-period of the applied voltage period, using a gate width of 45 µs for 10 kHz and 8 µs for 60 kHz discharges. As detailed above, these images were taken from the top of the discharge through a transparent electrode. Unless otherwise specified, camera properties remain fixed for every

image presented (one image per exposure, identical intensity multiplier for each). Multiple analyses were taken looking through the cathode (the negative current half-period) and through the anode (the positive current half-period) to analyze how one current alternance varies visually in regard to the other current alternance. A Keyence VHX-1000 Optical Microscope was used to analyze the surface of the MFC foams before and after plasma treatment. The microscope was used to analyze the surface area and the characteristic size of the damages produced by the plasma, as well as their distribution over the foam's surface.

3.2.3 - Experimental results and discussion

3.2.3.1 - Influence of the applied voltage frequency

The interaction between the DBD and the MFC foams was analyzed using different frequencies of the applied voltage. Considering the results of Levasseur *et al.* on porous wood samples [32], the MFC foams were first outgassed in the reactor chamber for 16 hours to remove as much as possible parasitic particles and/or gaseous species trapped inside the foam microstructure. Figure 14 presents the current-charge-voltage characteristics obtained at 10 kHz for an outgassed MFC foam. For the sake of brevity, three different time intervals are presented over the total plasma treatment time (60 min). The discharge current (red line) presents an irregular shape formed by a multitude of spikes randomly distributed in time. This is observed for each half-period of the applied voltage (black line) during about 20 µs. The presence of the spikes corresponds to the increase of the charge (charge build-up – blue line) in the discharge. When the charge reaches its maximum value, the current rapidly decreases to zero. Such current features are associated with a filamentary regime [53]. It must be noted, however, that the current shape changes as the plasma treatment time increases, suggesting a progressive modification of the discharge regime [10,46,53,84]. Similarly, the charge intensity increases from 2 to 60 min, leading to an increase of the discharge power, from 0.7 W at 2 min to 1.1 W at 60 min.

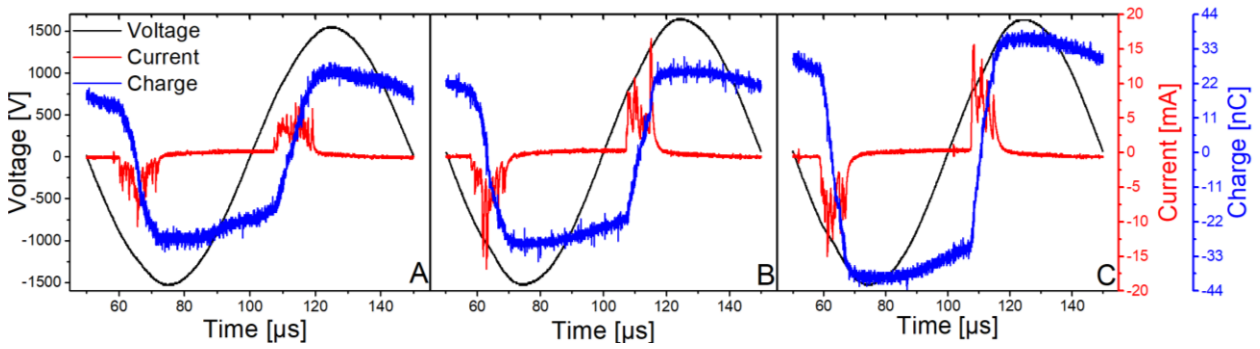

Figure 14. – I-Q-V measurements of a plane-to-plane DBD at 10 kHz with an outgassed MFC foam at different times over the total 60-min plasma treatment time: A) 2 min, B) 30 min, and C) 60 min.

In order to analyze the influence of the frequency on the discharge properties, Figure 15 shows the current-charge-voltage characteristics obtained at 60 kHz for an outgassed MFC foam. When the frequency increases, the shape of the discharge current changes and the amplitude increases. At 2 min, the discharge current (red line) presents a single peak per each half-cycle of the applied voltage with a discharge-on time of about 4 µs. Current peak intensity slightly increases with plasma treatment time, from 85 mA at 2 min to 120 mA after 60 min. As for the charge (blue line), it reaches a maximum value in less than 4 µs for each half-cycle of the applied voltage. The amplitude of the charge also increases between 2 min and 60 min of the plasma treatment. The current curves presented in Figure 15 are akin to a homogeneous, glow-like discharge regime [53]. This point must, however, be verified by fast imaging (see additional details below). It must be noted that a small bump also appears after the main discharge current peak; this could result from a second breakdown occurring after the first discharge because of the continuous increase of the gas voltage up to values higher than the breakdown voltage [47,85]. Under such conditions, the discharge power rises from 4.1 W at 2 min to 5.1 W at 60 min.

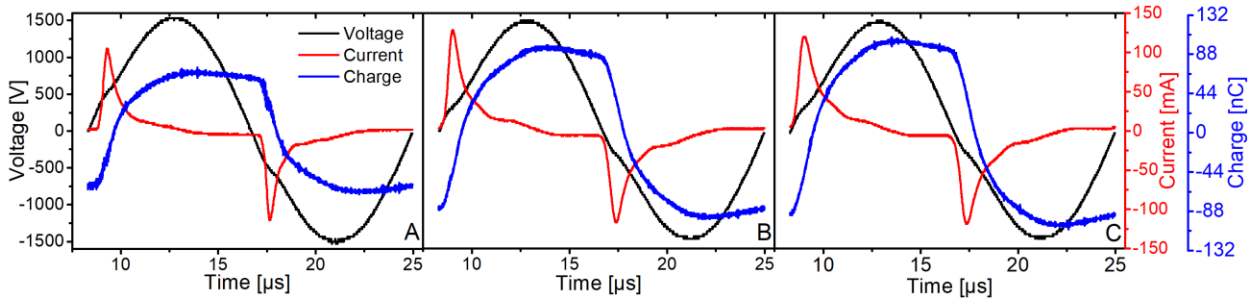

Figure 15. – I-Q-V measurements of a plane-to-plane DBD at 60 kHz with an outgassed MFC foam at different times over the total 60-min plasma treatment time: A) 2 min, B) 30 min, and C) 60 min.

According to the electrical measurements, the increase in frequency from 10 to 60 kHz (and thus the decrease in the discharge-off time between each half-cycle of the applied voltage) contribute to the development of an apparent glow-like regime even for very short plasma treatment times. Massines and her collaborators have studied the transition from a filamentary-like discharge to a homogeneous glow discharge in DBDs and have highlighted the importance of the so-called memory effect [44–46]. The authors have noted that the long-lived energetic species (*i.e.* metastable species, positive ions, etc.) can be "trapped" in the gas gap volume between each half-cycle of the applied voltage such that they can promote Townsend breakdown (leading to the homogeneous regime) rather than streamer breakdown (leading to the filamentary regime) from one half-cycle of the applied voltage to the other. At 60 kHz, the discharge-off time is approximately 5 µs, almost six times shorter than at 10 kHz (~40 µs). For plane-to-plane DBDs operated in nominally high-purity helium with an inter-electrode distance of 3 mm and a laminar gas flow, current-voltage characteristics typically reveal a homogeneous regime even at 10 kHz [32,34]. This reveals that the presence of an outgassed MFC foam alters the lifetime of energetic species such that it becomes shorter than about 40 µs. This could be due to the release of species involved in quenching reactions or the change in the gas flow dynamics (for example a transition from laminar to turbulent flow) with respect to plane-to-plane DBDs without MFC foam taking up the entirety of the gas gap. It could also affect the breakdown

dynamics due to the strongly inhomogeneous nature of the electric field with the highly porous MFC structure.

Figure 16 presents an optical microscope image of MFC foams after 60-min plasma treatments at either 10 or 60 kHz for outgassed samples. Figure 16A reveals that at 10 kHz the surface maintains its integrity after treatment such that the cellulosic fibers remain sparsely spread out throughout the MFC foam. Very similar images were obtained before plasma treatment (not shown). Only a few dispersed defects are visible after plasma treatment at 10 kHz, and they remain difficult to distinguish by the naked eye. A zoom over many damaged regions (see, for example, Figure 16B) highlights a typical defect size in the 0.1 mm^2 range (hole diameter ~0.4 mm). These were measured using an optical microscope. Similar damaged zones have been observed on wooden substrates with circular burns of the size of the discharge filaments (0.1 to 0.4 mm) [32,54,55]. Figure 16C presents the surface of the outgassed MFC foams subjected to a 60 kHz discharge. Significant plasma-induced damage, easily distinguishable by the naked eye, can be seen. Damage is uniformly distributed across the entire sample with a typical size of ~1.6 mm^2 (hole diameter ~1.7 mm). Such damages are not limited to the topmost surface but rather extend from one surface to the other (through-holes). When comparing the results obtained at different frequencies, one can note that the typical area (and diameter) of the holes changes considerably. With an outgassed MFC foam subjected to a 10 kHz discharge, the holes are over 15 times smaller on average than for 60 kHz discharge (see Figure 16). In addition, more damage is found at 60 kHz, which seems in contradiction with the glow-like aspect of the discharge claimed from current-voltage characteristics (see Figures 15). At this point it is important to highlight, however, that the power injected into the discharge was much lower at 10 kHz than at 60 kHz (current 10× less at 10 kHz than at 60 kHz, see Figures 14 and 15). Hence, more severe plasma-induced damage seems linked to increased number densities of charged species (ions, electrons, and excited states) and enhanced neutral gas heating as the frequency increases from 10 to 60 kHz [86].

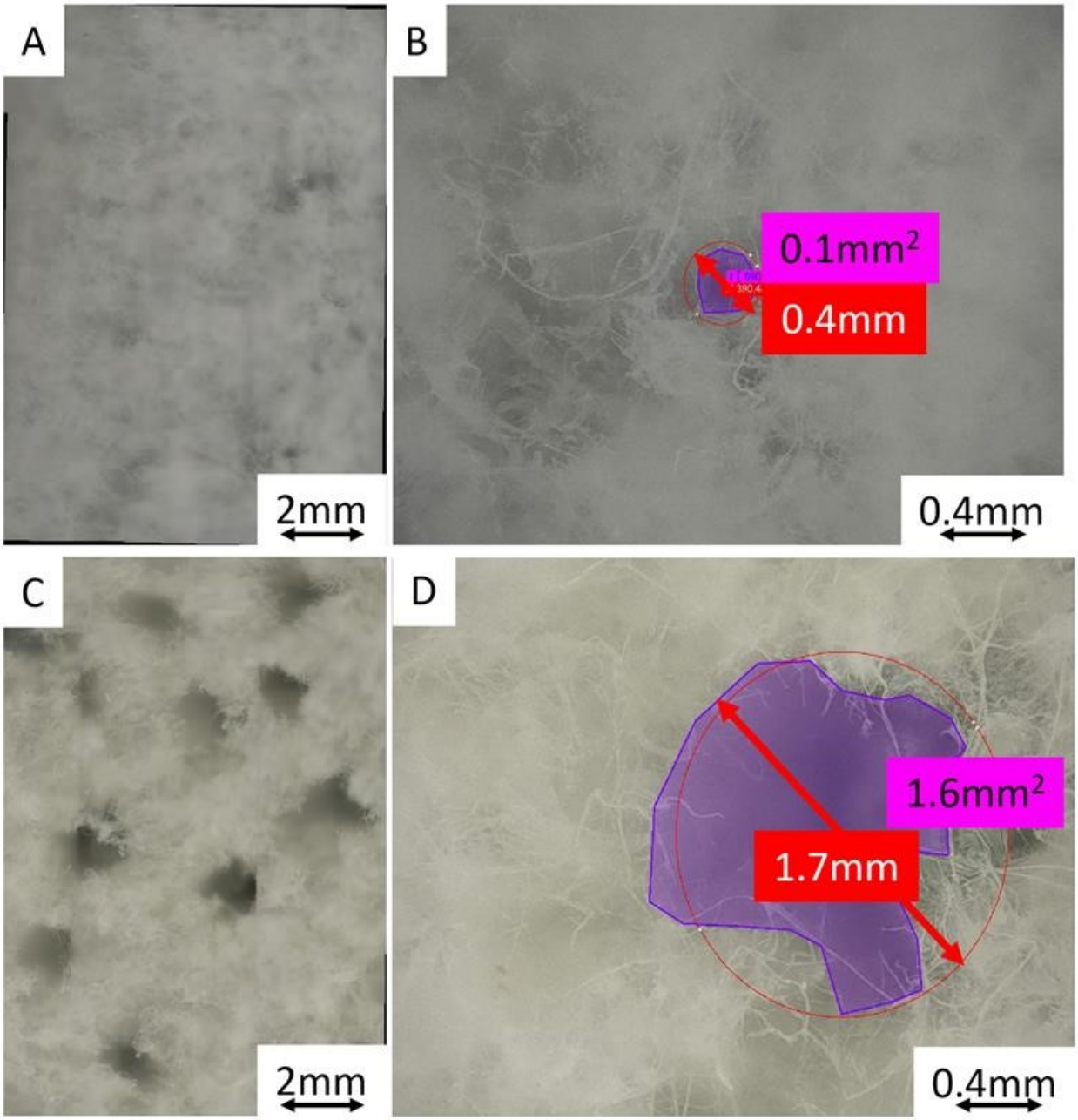

Figure 16. – Optical microscope images of the surface of the outgassed MFC foams after plasma treatment. A) Overall view of the surface; 10 kHz discharge. B) Close-up of a hole created by the presence of a filament; 10 kHz discharge (diameter: ≈ 0.4 mm, surface area: ≈ 0.1 mm^2). C) Overall view of the surface; 60 kHz discharge. D) Close-up of a hole created by the presence of a filament; 60 kHz discharge (diameter: ≈ 1.7 mm, surface area: ≈ 1.6 mm^2).

Electrical measurements do not offer a definitive proof of a discharge regime: light emission analysis are also required to draw such a conclusion [10]. High-speed camera images though a transparent electrode were therefore recorded during the interaction of the discharge with the outgassed MFC foam. Figure 17 shows the discharge light emission intensities from the top electrode captured during a single half-period of the applied voltage (the transparent electrode is the cathode). The results are presented for both frequencies, 10 kHz (A, B, and C) and 60 kHz (D, E, F), at different times over the total 60-min plasma treatment.

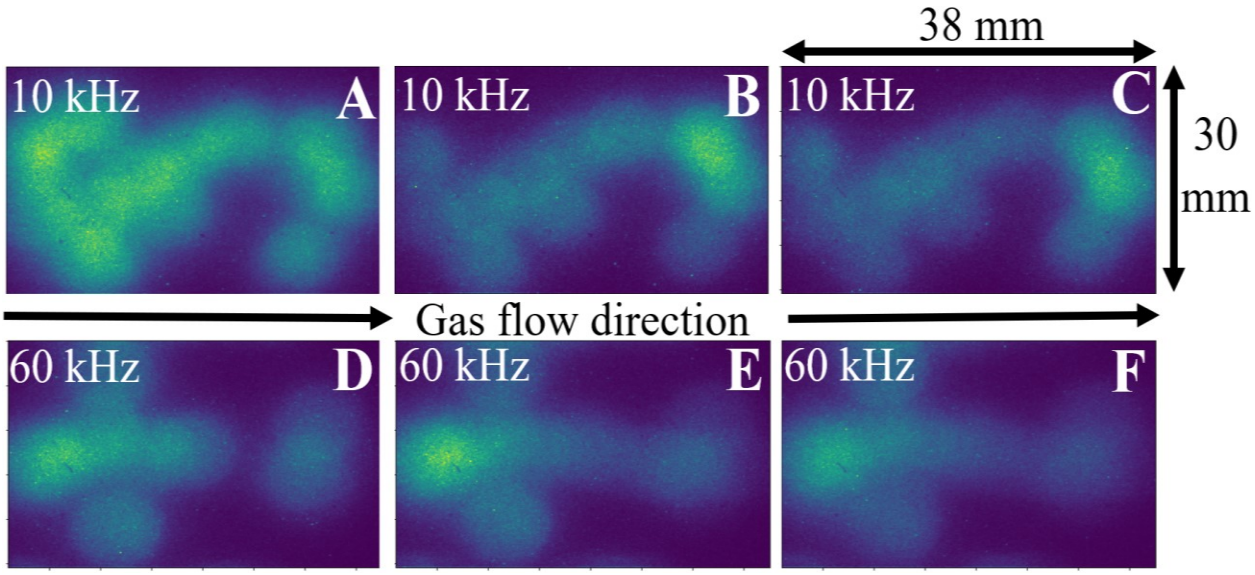

Figure 17. – ICCD image captures of the outgassed MFC foams subjected to a discharge at three different time intervals in order to observe potential time-based variations in light emissions patterns. For brevity, only the negative current alternance is shown (looking through the cathode). Similar results were obtained on the positive current alternance (looking through the anode). 10 kHz discharge – Gate width 45 µs – A) 5 min, B) 30 min, C) 60 min. 60 kHz discharge – Gate width 8 µs – D) 5 min, E) 30 min, F) 60 min.

At both 10 and 60 kHz, the discharge light emission does not cover the entire electrode region: most of the light emission intensity remains localized in specific regions of the outgassed MFC foam. By comparing the results obtained just after the breakdown (Figures 17A and 17D) with the ones obtained after 30 min (Figures 17B and 17E) and 60 min (Figures 17C and 17F), one can see that light emission patterns always come from the same area. Hence, the discharge first

ignites in a selected region of the MFC foam and then remains localized in that zone throughout the duration of the plasma treatment. In previous studies realized in presence of wood substrates placed on the bottom electrode of the plane-to-plane DBD with a gas gap between the wood surface and the top electrode, the structural inhomogeneities of the wooden materials produced non-uniform light emission patterns while maintaining homogeneous-like current-voltage characteristics [87]. Based on a simple electrical model of the discharge, this localization was ascribed to a change of the relative dielectric permittivity on 'early' versus 'late' wood affecting the local voltage applied to the gas, and thus the local discharge current [82]. In line with this study, discharge breakdown seems to first occur through fragile zones of the MFC foam where the local relative permittivity is lower (porosity is higher). This conclusion is consistent with the presence of holes in the MFC foams after plasma treatment (see Figure 16). However, emission spots are typically much larger than plasma-induced damage. For example, at 60 kHz, emission spots are in the 10-mm range whereas plasma-induced damage (holes) are in the 2-mm range. This indicates that light emission extends beyond the damage domain. This aspect is even more pronounced at 10 kHz, where emission spots are in the 10-mm range, whereas filaments and plasma-induced damage are in the 0.4-mm range.

At 10 kHz, Figure 17 further reveals that the light emission intensity sharply decreases between 5 and 30 min and then remains more or less constant between 30 and 60 min. This behavior is consistent with the transition from the heavy-filamentary regime to a less-filamentary regime with increasing plasma treatment time (see Figure 15) [10,46]. At 60 kHz, changes in the light emission intensities between 0 and 60 min are much less significant, in very good agreement with the very small modification in the current-voltage characteristics observed with increasing plasma treatment time (see Figure 16). When comparing the results obtained at different frequencies, one can note similar light emission intensities. Considering the difference in gate widths during snapshot images (45 µs at 10 kHz and 8 µs at 60 kHz), this indicates a lower population of excited species at 10 kHz than at 60 kHz, in very good agreement with electrical measurements (current 10× less at 10 kHz than at 60 kHz, see Figures 14 and 15).

High-speed camera images were also recorded through the side looking into the gas gap. Here, the gate width was fixed at 45 ns at 10 kHz and 16 ns at 60 kHz and measurements were recorded over the whole period of the applied voltage (100 µs for 10 kHz and 16 µs for 60 kHz). Selected images recorded at 2 min over the total 60-min plasma treatment are shown in Figure 18. For both 10 and 60 kHz conditions, images are displayed at the point of discharge ignition (A-10 kHz and C-60 kHz) and at the point of maximum discharge current (B-10 kHz and D-60 kHz). As described before, the discharge behavior is completely different for the two studied frequencies. At 10 kHz, the discharge is characterized by localized "randomly" distributed light spots; the discharge is filamentary. At 60 kHz, the discharge seems more diffuse (glow-like regime). In both cases, the discharge progagation mostly occurs through the foam from one electrode to the other. This reveals a volume discharge rather than a surface discharge [88].

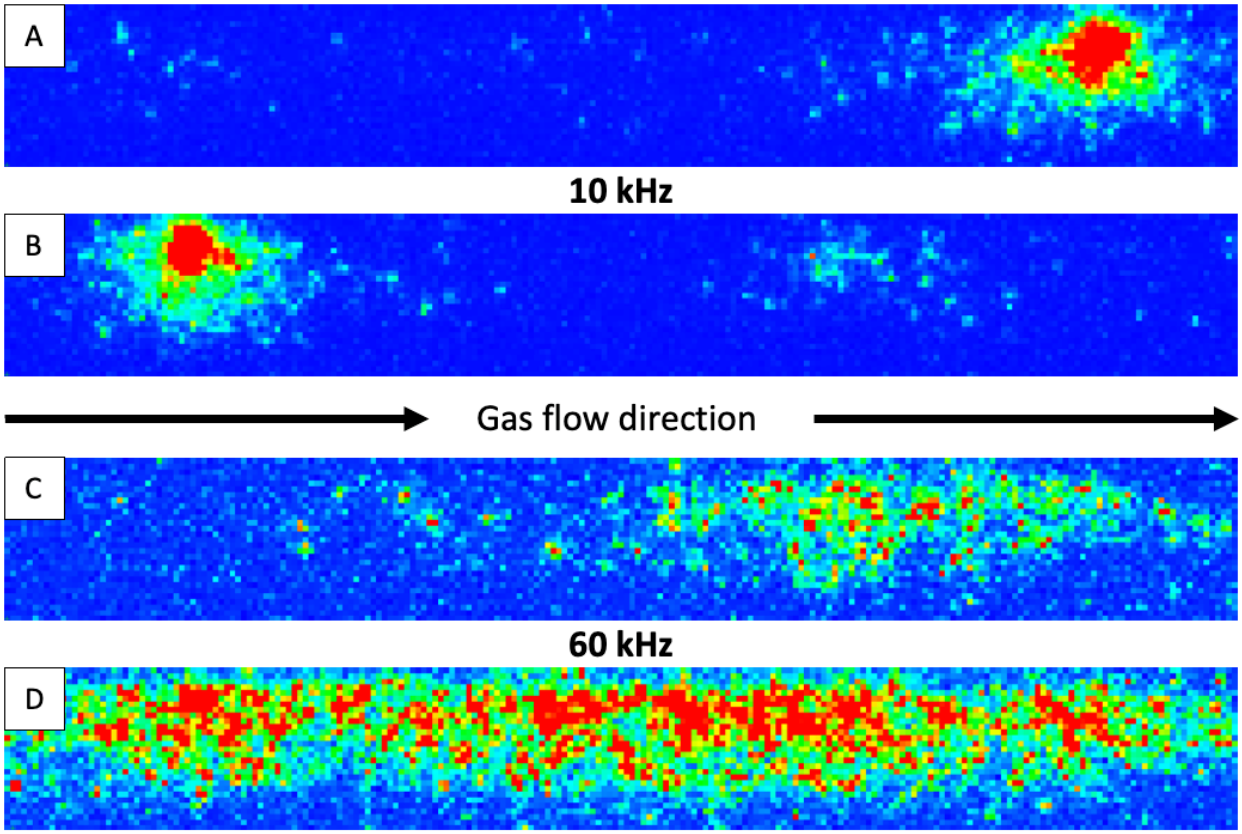

Figure 18. – ICCD image of the MFC foam recorded through the side looking into the gas gap. For brevity, only the positive current alternance is shown (top electrode is anode and bottom electrode is cathode). Similar results were obtained on the negative current alternance (top electrode is cathode and bottom electrode is anode). 10 kHz discharge – Gate width 45 ns – A) discharge ignition point (low discharge current) and B) discharge propagation point (maximum discharge current). 60 kHz discharge – Gate width 16 ns – C) discharge ignition point (low discharge current) and D) discharge propagation point (maximum discharge current).

3.2.3.2 - Influence of substrate outgassing

Outgassing from porous substrates during materials processing has a very consequential effect on the physical characteristics of DBD. For example, Levasseur *et al.* have demonstrated that outgassing phenomena during plasma processing of wood substrates can not only modify the discharge regime (transition from filamentary to glow-like), but can also alter the physico-chemical properties of plasma-deposited coatings [49]. The authors have further shown that

residual gaseous species trapped in the wood microstructure and released from the plasma-wood interaction significantly modify the electron energy reservoir (electron density and temperature) and the population of long-lived metastable species [46]. It must be noted that these measurements were realized with the wood sample placed on the bottom DBD electrode and with a gas gap of a few mm between the wood's topmost surface and the top DBD electrode. Here, the MFC foam occupies the entire gas gap volume. In addition, the difference in porosity between these ligno-cellulosic samples implies different absorption/desorption rates of impurities in the nominally high-purity He plasma [32,50]. Figure 19 presents the electrical characteristic of the discharge obtained with non-outgassed MFC foams.

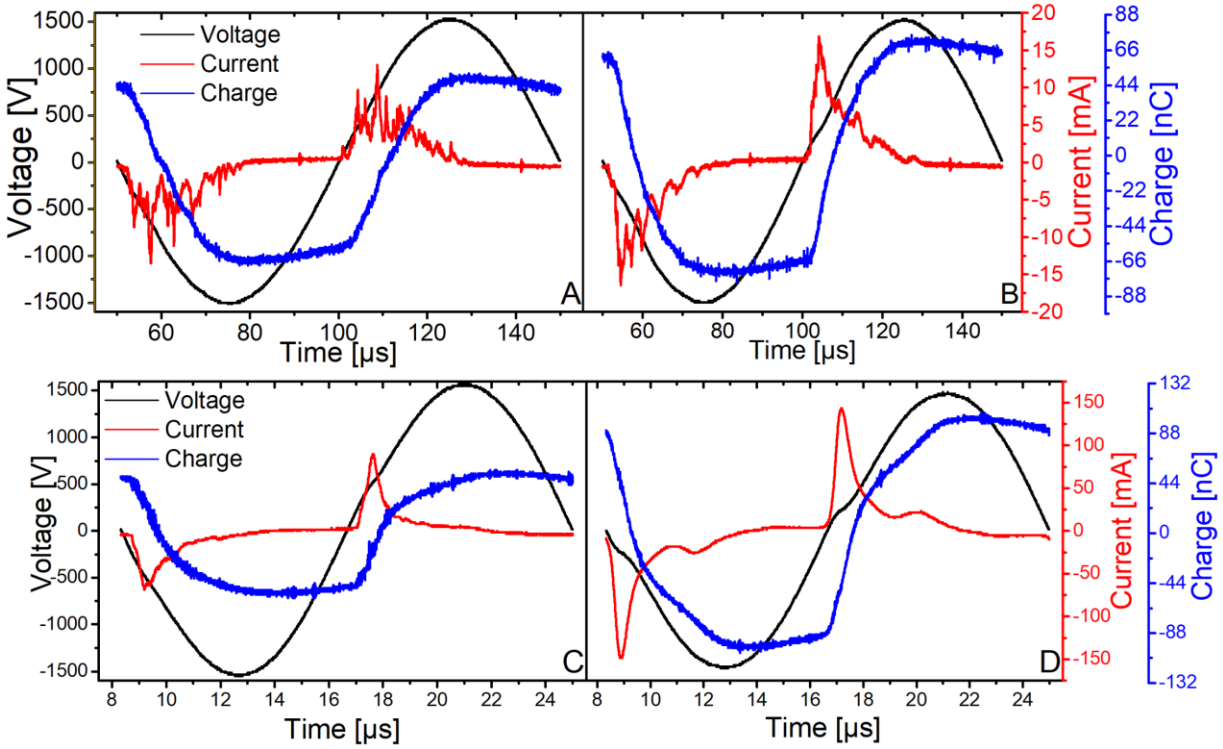

Figure 19. – I-Q-V curves of the non-outgassed MFC foams subjected to a 10 kHz discharge at A) 2 min and B) 60 min, and to a 60 kHz discharge at C) 2 min and D) 60 min.

For the MFC foams subjected to a 10 kHz discharge, a multitude of current peaks randomly distributed in time are observed over the whole range of plasma treatment times examined (Figures 19A and 19B). As previously explained, this is akin to a filamentary discharge regime [53]. In such conditions, the discharge power increases from 1.4 W at 2 min to 1.6 W at 60 min. As expected, these values, obtained in the presence of impurities in the nominally high-purity He plasma, are higher than those obtained for outgassed samples [32]. This aspect is better illustrated in Figure 20. It is interesting to note that the higher power densities achieved with outgassing than without outgassing remain even after a 1-h plasma treatment [49]. This is inherent to the very low "pumping rates" of the helium gas flow going through the sample when the MFC foam occupies the entire gas gap volume. At 60 kHz, the data captured in the first two minutes of the plasma treatment (2 min, Figure 19C) has an overall smaller current measurement than the other (60 min, Figure 19D), with a peak value around 100 mA. As time goes on, the current peak increases to approximately 150 mA. In all cases, the electrical signals suggest a homogeneous discharge regime. It is of note that the presence of a second breakdown after the main discharge current peak remains observable under non-outgassed conditions. In addition, the slight bump after the main current peak is more pronounced in presence of outgassing impurities than in outgassed conditions. This is consistent with the results reported in the literature for nominally high-purity He DBD in presence of Ar admixtures [85]. Similar variations are observed in charge measurements. Here, as shown in Figure 20, the discharge power rises from 7.2 W at 2 min to 9.6 W at 60 min.

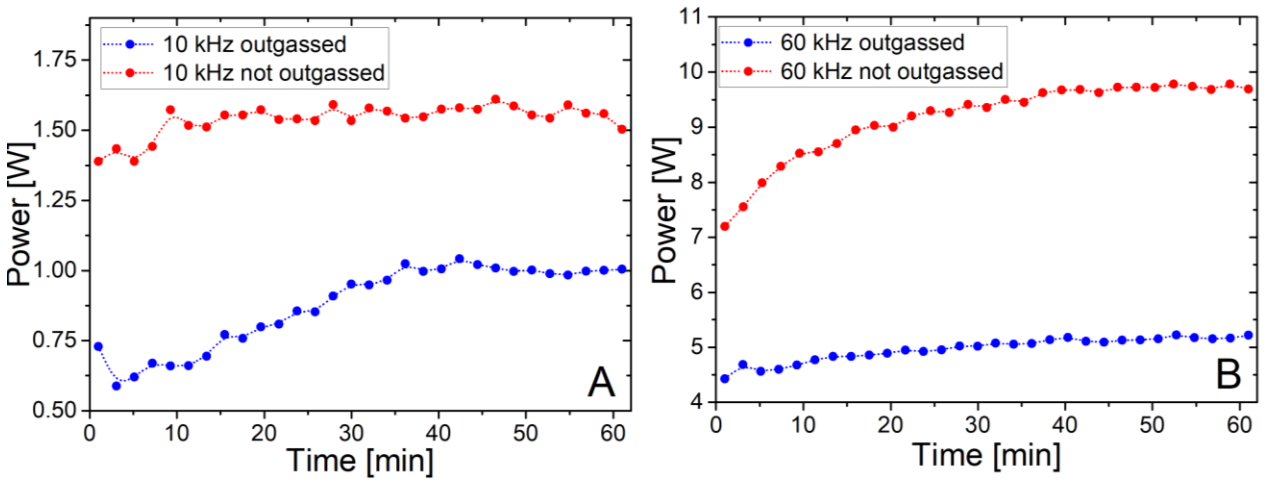

Figure 20. – Power dissipated in the DBD as a function of plasma treatment time of both outgassed and non-outgassed MFC foams subjected to A) a 10 kHz discharge and B) a 60 kHz discharge.

Figure 21 presents optical microscope images of the surface of non-outgassed MFC foams subjected to either a 10 kHz (A and B) or 60 kHz (C and D) discharges. At both frequencies, plasma-induced damage is more pronounced in non-outgassed conditions (Figure 21) than in outgassed conditions (Figure 16). More specifically, the typical hole diameter and surface area are 1.2 mm and 0.6 mm^2 at 10 kHz, increasing to 2.5 mm and 3.3 mm^2 at 60 kHz. This indicates that substrate outgassing prior to the plasma treatment strongly influences plasma-induced modification of the MFC foams. This can most likely be ascribed to the erosion of ligno-cellulosic materials in presence of air (and thus oxygen) impurities [35,36,89].

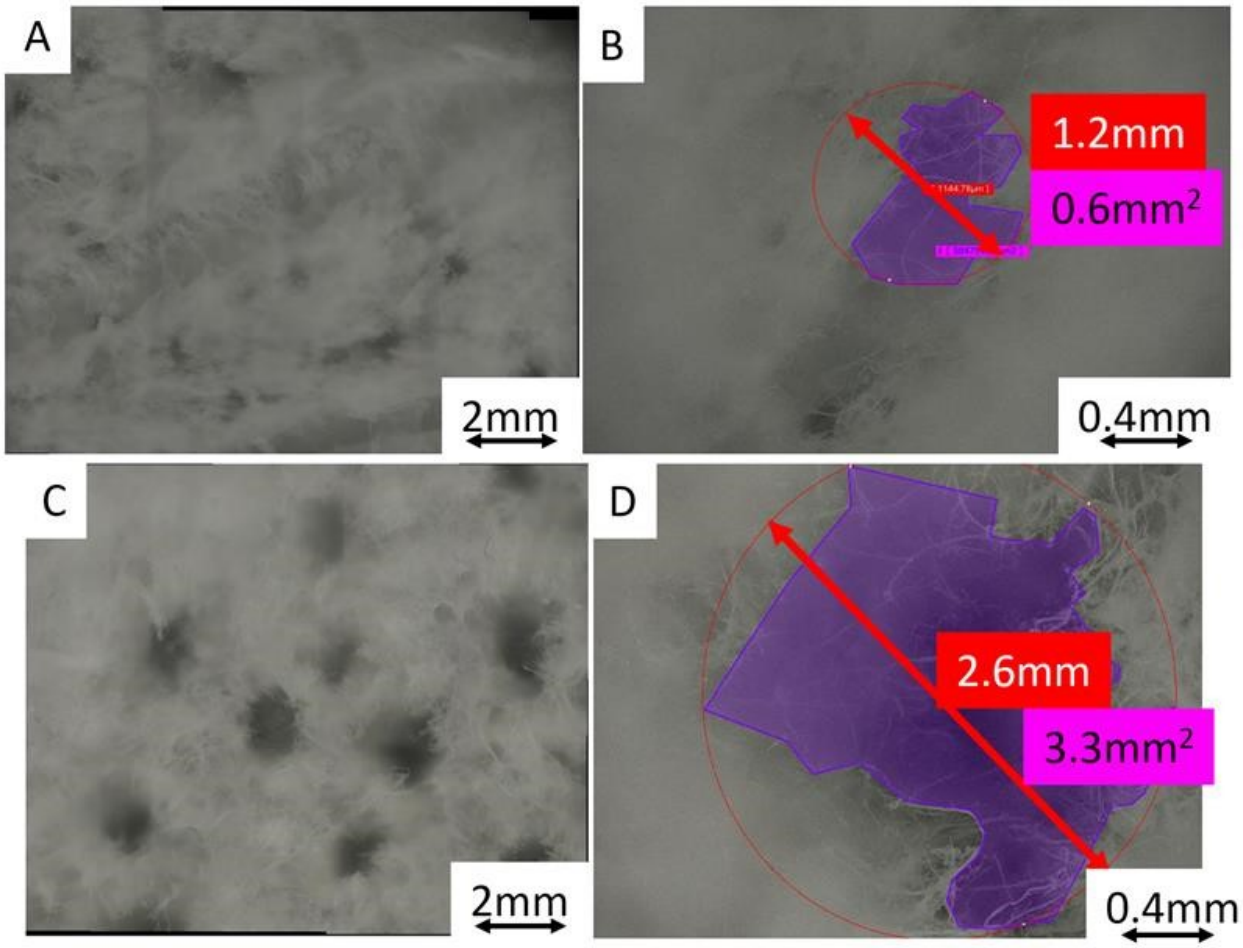

Figure 21. – Optical microscope images of the surface of the non-outgassed MFC foams after plasma treatment. A) Overall view of the surface; 10 kHz discharge. B) Close-up of a hole created by the presence of a filament; 10 kHz discharge (diameter: ≈ 1.2 mm, surface area: ≈ 0.6 mm^2). C) Overall view of the surface; 60 kHz discharge. D) Close-up of a hole created by the presence of a filament; 60 kHz discharge (diameter: ≈ 2.6 mm, surface area: ≈ 3.3 mm^2

Light emission patterns from the top electrode captured during a single half-period of the applied voltage (the transparent electrode is cathode) for non-outgassed MFC foams are shown in Figure 22. At 10 kHz (Figure 22A through 22B), similar phenomena to those occurring in outgassed MFC foams are observed. The breakdown remains localized and the formation of preferential discharge canals is again observed. Interestingly, the size of the emitting spots (~5-7 mm) is again larger than the diameter of plasma-induced damage (~2.6 mm). However, the

number of emitting spots is much higher than in outgassed conditions (Figures 22A and 22B versus Figures 17A, 17B, and 17C), which is consistent with more prominent damage (Figures 21A versus Figure 16A). On the other hand, at 60 kHz, the discharge presents a different temporally-defined phenomenon. Here, the discharge appears very homogeneous (Figure 22B), with only minor intensity variations across the whole zone probed by the ICCD camera. Considering the enhanced damage formation dynamics at 60 kHz compared to 10 kHz and in non-outgassed versus outgassed conditions, it seems that the local emitting spots begin to overlap, giving rise to an apparent homogeneous light emission at the scale of the ICCD measurement (gate width of 8 µs at 60 kHz). Again, discharge propagation occurs through the foam from one electrode to the other (volume discharge).

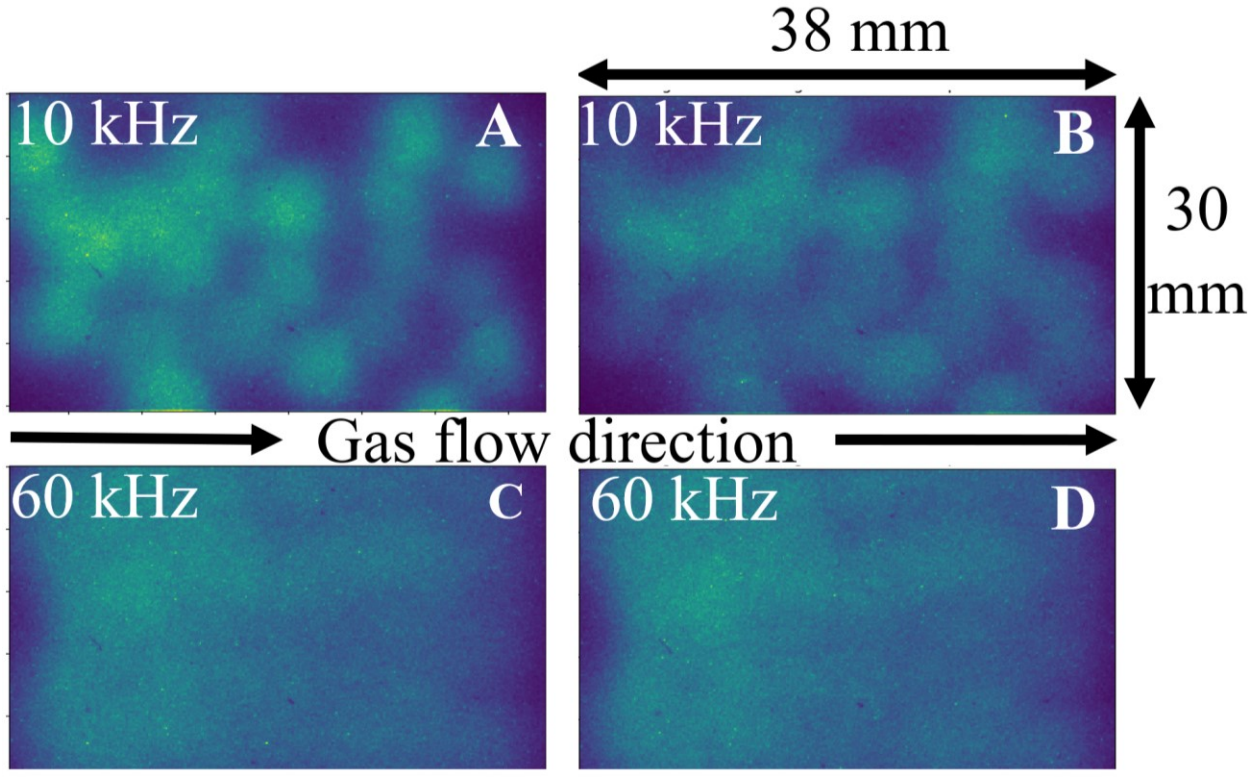

Figure 22. – ICCD image captures of the non-outgassed MFC foams subjected to a discharge at two different time intervals in order to observe potential time-based variations in light emissions patterns. For brevity, only the negative current alternance is shown (looking through the cathode). 10 kHz discharge – Gate width 45 µs – A) 5 min, B) 60 min. 60 kHz discharge – Gate width 8 µs – C) 5 min, D) 60 min.

During plasma treatment of materials of bulk, wood samples, outgassing phenomena typically vanished with increasing plasma treatment time due to the “entire” release of air impurities [49]. At such conditions, the discharge power for non-outgassed samples was very high early in the plasma treatment and then decreased to the value observed for outgassed samples with increasing plasma treatment time [32]. Clearly, this is not observed in Figure 20. More specifically, for MFC foams, the power density continuously rises with plasma treatment time despite the expected decrease of outgassing effects. Based on the results presented in Figures 16 and 17 for outgassed samples, and Figures 21 and 22 for non-outgassed samples, this discrepancy is linked to the formation of plasma-induced damage that increases the plasma volume and thus the power dissipated in the discharge. Hence, the trends observed in Figure 20 reflect both outgassing (which would lead to a decrease of the power with time) and plasma-induced damage formation (which would lead to an increase of the power with time).

3.2.4 - Conclusion

In summary, this work describes the fundamental discharge phenomena that occur when a complex, porous, wood-derived, microfibrillated cellulose foam occupies the entirety of the gas gap of a plane-to-plane helium DBD at atmospheric pressure. The different discharge conditions and configurations were analyzed primarily at two different frequencies, 10 and 60 kHz, using both outgassed and non-outgassed MFC foams. Electrical, microscopic, and optical emission spectroscopy measurements were made to ascertain a general global understanding of the discharge properties when operated in this unique configuration. It was found that discharge ignition and propagation mostly occurs through the foam from one electrode to the other (volume discharge). In addition, higher frequencies generated higher power outputs than lower frequency discharges, and that higher frequencies also encouraged greater damage developments in the foam. It was also found that outgassing a substrate before subjecting it to the discharge not only reduced the power output of the discharge, but also reduced damage incurred by said foam. For fully-outgassed foams, electrical and optical measurements revealed a glow-like discharge regime at 60 kHz and a filamentary behaviour at 10 kHz. This work can be

used as building blocks for the functionalization of wood-derived microfibrillated cellulose foam for technological applications, for example to enhance its water repellence by plasma deposition using non-toxic organosilicon precursor molecules [50].

3.2.5 - Acknowledgments

This work was financially supported by the National Science and Engineering Research Council (NSERC), PRIMA-Québec, Plasmionique inc., and FPInnovations. Louis-Félix Meunier acknowledges Mitacs Globalink, the Direction des Relations Internationales of the Université de Montréal, and Université Paul-Sabatier de Toulouse for their support to the Québec-France student exchange master program.

3.3 - Modification of Microfibrillated Cellulosic Foams in a Dielectric Barrier Discharge at Atmospheric Pressure

Louis-Félix Meunier[1,2], Jacopo Profili[1], Sara Babaei[1], Siavash Asadollahi[3], Andranik Sarkissian[3], Annie Dorris,[4] Stephanie Beck, Nicolas Naudé[2], and Luc Stafford[13]

[1]*Département de physique, Université de Montréal, Montréal, Québec, H2V 0B3, Canada*

[2]*LAPLACE - Laboratoire Plasma et Conversion d'Énergie, Université Paul Sabatier, Toulouse, 31062, France*

[3]*Plasmionique Inc., Varennes, Québec, J3X 1S2, Canada*

[4]*FPInnovations, Pointe-Claire, Québec, H9R 3J9, Canada*

ABSTRACT

This work explores the plasma-induced modification of microfibrillated cellulose (MFC) foams in a plane-to-plane atmospheric-pressure dielectric barrier discharge with helium and hexamethyldisiloxane as carrier and precursor gases, with and without a gas gap. When the foam took up all of the gas gap, filamentary discharges were generated and produced burn-like damage. This produced highly inhomogeneous deposits having both hydrophilic and hydrophobic domains. MFC foams taking up only a portion of the gas gap volume generated a homogeneous discharge and induced cellulose defibrillation. They generated effective hydrophobic surfaces on both the top and bottom of the foams. Oleophilicity measurements were also carried out and support the possibility of an effective separation of oily wastewater using a green and renewable material.

KEYWORDS: Cellulose, dielectric barrier discharge, plasma deposition, hydrophobicity, oleophilicity, selective adsorption

[3] Electronic mail: luc.stafford@umontreal.ca

3.3.1 - Introduction

Every year, a large volume of oily wastewater is produced from various industries, such as food packaging industries, petroleum refineries, vegetable oil and hydrogenated oil manufacturing, and the metallurgic industries [15]. The low degradability of most oily products in nature as well as their complex and toxic composition strongly affect our biosphere [15,16]. For this reason, release of oily substances into water by industry is increasingly regulated and different processes have been implemented to mitigate and prevent deleterious effects on the environment [15,17]. With respect to oil-water separation, traditional techniques include oil-water emulsion with air flotation [18], flocculation [19], and oil skimming [20]. While the employment of these techniques is relatively well documented, their use remains costly and has relatively low separation efficiency [21]. Alternative methods to decontaminate water streams have been studied in the literature, including innovative and modified porous materials, which have been suggested as a possible passive solution [57]. These products must selectively absorb oil and not interact with water. As an example, authors have obtained good oil-water separation properties by coating stainless steel with conductive polymers [21], by adding polyacrylamide hydrogels onto metals [90], by modifying copper grids with perfluoroalkylsilanes [91] or by mixing organic precursors with inorganic nanoparticles [92]. However, most of these approaches have a high environmental impact because of the oil-based substrates and materials used.

To respect environmental restrictions, many industries are now considering the use of bio-based products for wastewater decontamination. In this context, Srinivasan *et al.* have shown how fungal biomass can be used to remove oil from water [58]. Unfortunately, the use of meshes and substrates issued from unmodified green products are often limited due to their natural hygroscopicity. [58,93,94]. Bio-based materials are therefore often functionalized to alter their chemical affinity [5–7,9,11,24,79,95]. Mansourizadeh *et al*. have developed hydrophilic and oleophobic membranes from blends of polyethersulfone/cellulose acetate by using a phase-inversion process. The authors have successfully shown selective adsorption properties and have demonstrated an oil-water separation with 88% efficiency [57]. Rohrbach *et al*. have generated cellulose paper filters modified with nanofibrillated cellulose (NFC) hydrogel to obtain a

separation efficiency greater than 99% [59]. Wang *et al*. synthesized cellulose sponges with superoleophobic and superhydrophilic properties for effective water-oil separation in underwater environments [60]. More recently, Lu *et al.* showed that cotton fabrics decorated with a combination of CuO deposition and stearic acid coating offered a robust and promising alternative to the existing water treatment, especially in oil/water separation [96].

While all the mentioned examples used bio-based materials, the hydrophobic and/or oleophobic layers were achieved using wet chemistry methods [11,13]. These techniques often require high amounts of chemical precursors, resulting in a high environmental impact. As a result, dry treatments such as non-thermal plasma approaches have recently gained significant traction. In this context, dielectric barrier discharges (DBD) at atmospheric pressure are one of the most adapted industrial techniques to modify these materials: the easy configuration (two electrodes separated by at least one dielectric) and the open-to-air configuration facilitate their use in industrial assembly lines. Large surfaces can also be treated rapidly without the need for expensive vacuum equipment [37,97]. Finally, the dielectrics limit the arc formation usually observed in atmospheric-pressure plasmas, allowing the surface modification of heat-sensitive bio-based materials without affecting their physical integrity [2,31,98].

Levasseur *et al.* [50,99] and Profili *et al.* [55,71] have demonstrated the possibility of using plane-to-plane DBDs to confer hydrophobic properties onto cellulosic (wood and paper) substrates. Both managed to alter the chemical response of the samples without incurring damage on their surfaces. Macedo *et al.* have modified cellulosic vegetable fibres in oxygen-containing plasmas at atmospheric pressure and have reported an improvement of the composite matrix filled with the modified fibres [100]. Garcia-Torres *et al.* have also reduced the water contact angle (WCA) of cellulosic substrates by a factor of two by plasma deposition of poly(acrylic acid) film in plasmas at atmospheric pressure [101]. It is also worth mentioning that Fanelli *et al*. have studied the modification of porous polyurethane foams with DBDs in order to favour the removal of heavy metal particle pollution from water sources [73,78]. To date, no work on the modification of porous bio-based foam in a DBD configuration has been reported in the literature.

In this work, we demonstrate the selective plasma modification of microfibrillated cellulose (MFC) foams derived from woody biomass by using a helium plasma discharge at atmospheric pressure and hexamethyldisiloxane (HMDSO) as the precursor for plasma deposition. The interaction of the plasma-treated surfaces with water and oil droplets is discussed. The role of the gas gap is further related to the hydrophobic and oleophilic properties of the surfaces.

3.3.2 - Experimental details

3.3.2.1 - Sample Preparation

MFC foams were prepared and provided by FPInnovations. Briefly, a suspension of cellulose microfibrils at 0.3wt% was lyophilized in a REVO85 freeze dryer from Millrock Technology. One must note that the specific concentration directly affects the density and porosity of the MFC material by using this type of process. Prior to plasma treatment, the MFC foams were cut into 75 mm × 65 mm rectangles.

3.3.2.2 - Plasma Treatment

The experimental setup for plasma treatment of MFC foams was a vacuum chamber containing a plane-to-plane DBD cell. Two alumina dielectrics were covered with a conductive paste to make the electrodes. Of note, the size of the MFC foams (75 mm × 65 mm) was big enough to ensure that they covered the entirety of the electrode surface area (65 mm × 55 mm). Glass shims were also placed along the sides of the dielectrics to direct gas flow into the inter-electrode gap. During the discharge, helium gas along with small amounts of HMDSO precursor liquid were continuously injected between the two dielectrics at a rate of 4.5 standard litres per minute (SLM) and 120 g/h, respectively. Light pumping was used to maintain atmospheric pressure inside the reactor chamber. The breakdown of the gas mixture was ensured by applying a sinusoidal voltage between the electrodes. A 20 kHz signal was sent then amplified using an audio power-amplifier (Crest Audio CC4000 Professional 4000) and a high-voltage transformer.

All samples were subjected to a discharge for 1 hour. Applied voltage and current flowing through the DBD cell were measured by a high voltage probe (Tektronix P6015A) and a wideband terminated current transformer (LILCO Ltd. 13W5000), respectively. The signals were then visualized using an oscilloscope (Tektronix TDS2014C 4 Channel Digital Storage Oscilloscope).

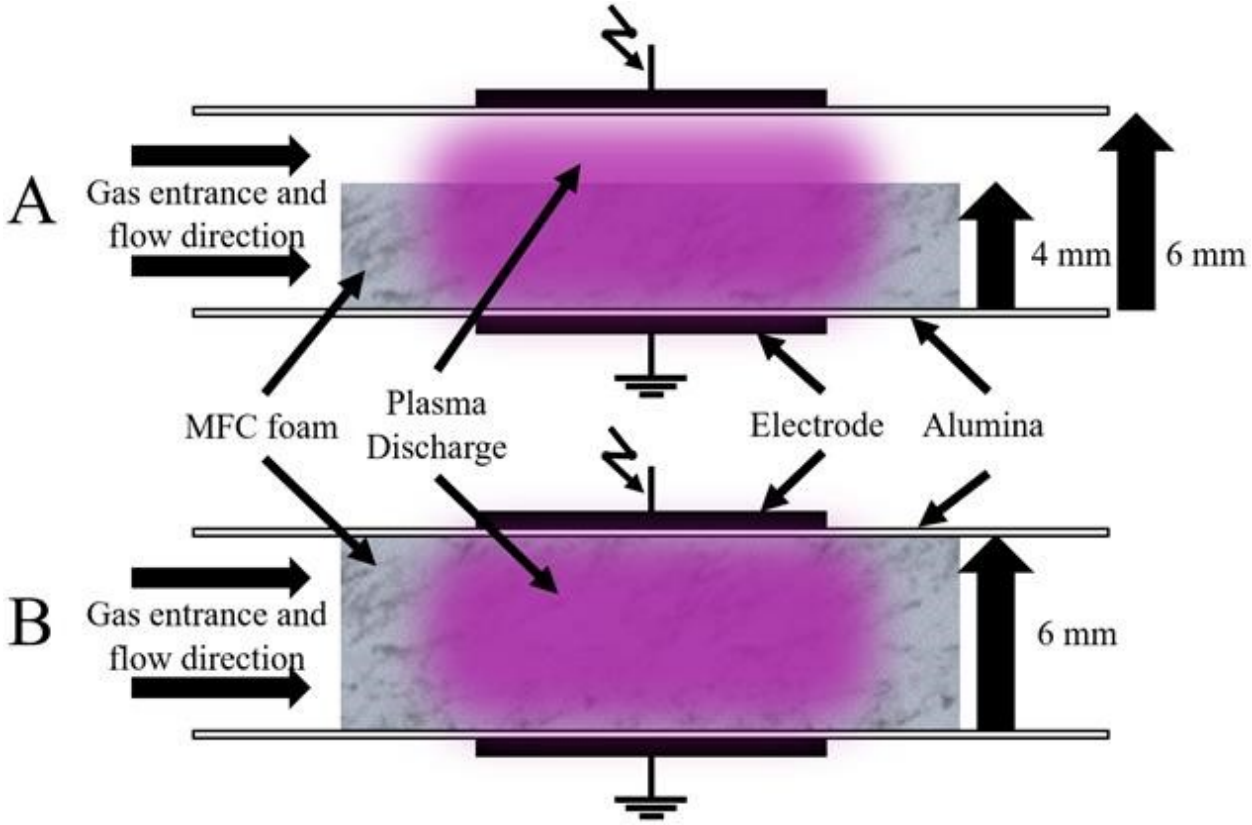

Figure 23. – Experimental setup used when (A) MFC foams occupy a portion of the gas gap volume and (B) MFC foams occupy the entirety of the gas gap volume.

The amplitude of the applied voltage was set at 3 kVpp when the MFC foams took up a portion of the gas gap volume (see Figure 23A) and 4 kVpp when they took up the entirety of the gas gap volume (see Figure 23B). In the first configuration (Figure 23A), the samples were secured to the bottom dielectric plate using Kapton tape along all four of its edges. Hence, the gas could flow on the surface and through the foam (within the topmost surface). With the second configuration (Figure 23B), the sample was maintained in place by the two dielectric plates. Thus, the gas flowed entirely through the foam. Hereafter, the first configuration where the foam takes a portion of the gas gap volume will be referred as the “gap”, and the second where the foam

takes up the entirety of the gas gap volume will be referred to as “no gap”. Prior to each plasma treatment, all the samples were outgassed at 20 mTorr for approximately 16 h in the vacuum chamber where the discharge takes place to ensure a minimal amount of impurities in the discharge, such as gas molecules issued from oxygen or humidity absorbed by the MFC foams [49,50,55].

3.3.2.3 - Surface Morphology and Chemistry

In order to have an extensive insight on the morphology of the substrates after the plasma treatment, scanning electron microscopy (SEM) analyses were carried out using a JSM-7600F scanning electron microscope equipped with a field emission (FE) electron emitter. Images were taken at 1 or 2 kV to minimize distortions and charging effects. Because of the fragility and the low electrical conductivity of the foam, images were taken at different locations on the foam surface. Surface chemistry was probed by using energy-dispersive X-ray spectroscopy (EDS). The EDS was used to map the chemical modifications of the foam before and after plasma treatment. These measurements were carried out at different accelerating voltages, *i.e.* 5 kV and 10 kV, to get a better understanding of the chemistry of both the topmost surface and the interior of the foam. Multiple EDS measurements were taken at different points on the foam to acquire a general chemical property mapping.

3.3.2.3 - Contact Angle Measurements

The substrates were subjected to wettability measurements in order to assess the extent of hydrophobicity and oleophilicity after plasma treatment. Hydrophobicity analyses were made through static water contact angle (WCA) measurements. A contact angle goniometer (OneAttension Theta, Biolin Scientific) was connected to a video camera system and computer software (Attension). Distilled water droplets (5 µL) were placed onto the substrate using a Sessile drop method. Static WCA and volume variation values were acquired over a 5-min time interval. The measurements were carried out at 6 different points on the MFC sample: two near the entrance, two in the middle portion of the foam, and two near the gas exit (here the entrance is

the region close to the gas injector). Oleophilicity measurements were done by manually adding a 5 µL droplet of Kerosene purum (Sigma-Aldrich, #STBJ0005) using a syringe. Static contact angle and droplet volume variations were captured using the same instrument and method as with the WCA measurements. Because of the distinct properties of oil and water, both liquids were manually and independently added onto the MFC foam surface.

3.3.3 - Experimental results and discussion

3.3.3.1 - Plasma Characterization

Current-voltage characteristics of the two experimental conditions (*i.e.* foam occupying either part of the gas gap volume or the entirety of the gas gap volume) were recorded at 2, 30 and 60 min of the 1-h plasma treatment time. The results are presented in Figures 24 and 25. Over time, current curves obtained from the first configuration (Figure 24) do not vary significantly and maintain a similar signature. The measured current curve exhibits two distinguishable regions: i) the sinusoidal portion, which is associated with the displacement current and ii) the broad peaks, which are associated with the discharge current. These current peaks are usually related in the literature to a homogeneous glow-like discharge regime [2,10,23,32,46].

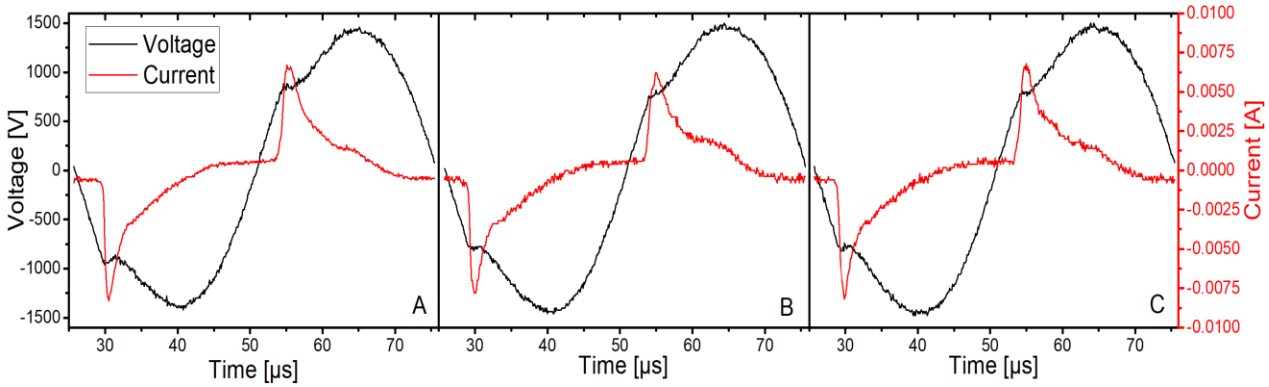

Figure 24. – Current-voltage characteristics of a plane-to-plane He-HMDSO dielectric barrier discharge with an outgassed MFC foam taking up a portion of the gas gap volume (corresponds to Figure 23A) at (A) 2 min, (B) 30 min, and (C) 60 min of the 1-h total plasma treatment time.

Similar experiments were realized with the foam taking up the entirety of the gas gap volume. Because of the "barrier" between the two dielectric plates induced by the porous MFC foam, the discharge had significant difficulty in maintaining a repeatable breakdown. For this reason, the amplitude of the applied voltage was increased from 3 to 4 kVpp. At such conditions, the current curves are consistently different from those displayed in Figure 24. More specifically, in Figure 25A, the signature of a homogeneous discharge (one current peak) is noticeable. However, the current remains polluted with parasitic breakdowns. As the discharge continues, filaments begin to appear, giving way to a few sharp current oscillations typically found in a filamentary regime (*i.e*. multiple current peaks randomly distributed in time and space [46,49]). This means that a mix of homogeneous and filamentary regime is observed when no gas gap is used. It must be noted that filamentary discharges can heavily damage the substrate [2,44,84]. For example, Profili *et al.* [55] observed a multitude of burns on bulk wood samples exposed to filamentary DBDs, with the damage diameter close to that of single microdischarges [55]. From the electrical measurements obtained in this work, one can also note that the discharge does not stabilize over time and remains filamentary.

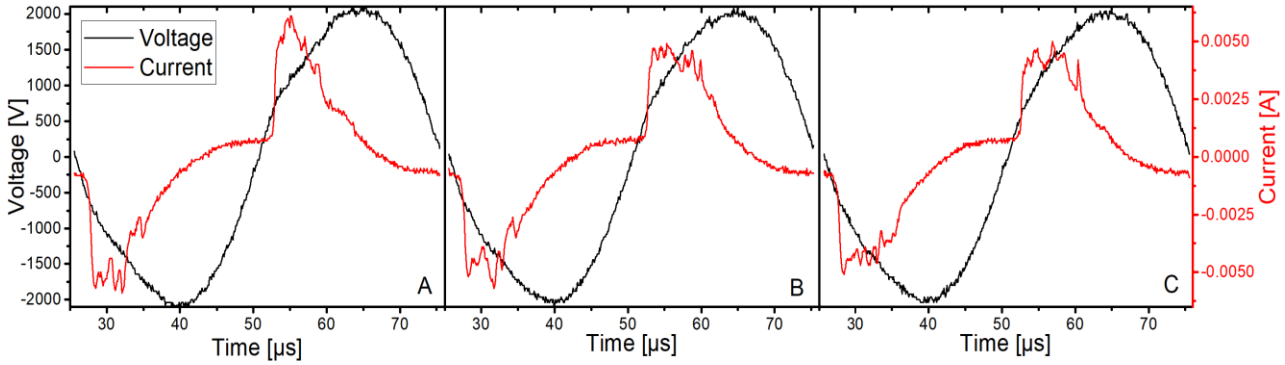

Figure 25. – Current-voltage characteristics of a plane-to-plane He-HMDSO dielectric barrier discharge with an outgassed MFC foam taking up the whole gas gap volume (corresponds to Figure 23B) at (A) 2 min, (B) 30 min, and (C) 60 min of the 1-hour total plasma treatment time.

Although the amplitude of the applied voltage is lower in Figure 24 than in Figure 25, current values obtained without the gas gap (Figure 25) remain smaller than the ones measured with the gas gap (Figure 24). When considering MFC foams taking up only a portion of the gas gap volume (configuration A in Figure 23), the power measured did not vary much throughout the entire hour of the plasma treatment, with values in the 100 W range. Assuming that the discharge is homogeneously distributed across the MFC foam surface, this corresponds to power density of 2.9 W/cm^2. When discharges took place without any gas gap (configuration B in Figure 23), power values were 160 W. In such conditions, the discharge is no longer homogeneously distributed, but rather localized in selected regions of the MFC foams [102]. Assuming that the discharge area corresponds to 20% of the surface area of the foam exposed to the applied voltage [102], this corresponds to power density of 22 W/cm^2. This greater power being highly localized in space, significant plasma-induced damage is expected, as shown below.

3.3.3.2 - Surface Morphology

Plasma-induced modification to the MFC foam was first examined by optical microscopy. Figure 26 presents the visual characteristics of the MFC foams after a 1-h plasma treatment in both configurations. The original colour of the foams before treatment was white. While foam

subjected to the configuration A did not exhibit major changes visible to the naked eye, retaining their pristine white colour, foam subjected to configuration B had multiple localized coloured spots staining the surface. These coloured spots have an approximate diameter of between 3 and 6 mm. Light superficial decohesion and the formation of small pores is observed in both cases.

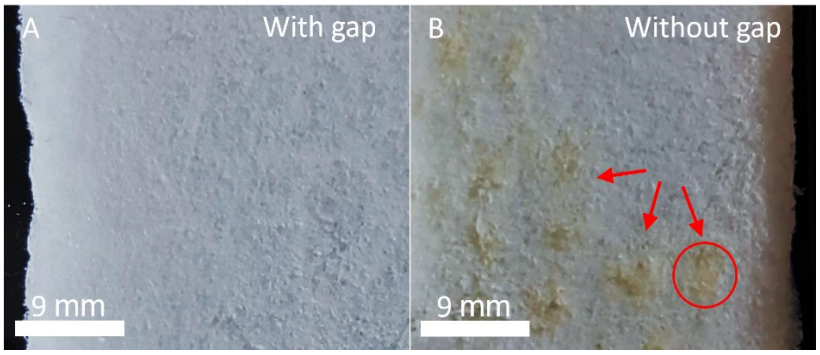

Figure 26. – Pictures of the surfaces of the MFC foam. (A) Foam taking up a portion of the gas gap volume with no visible discolouration. (B) Foam taking up the entirety of the gas gap volume with visible yellow stained on its surface.

SEM images were also recorded to investigate the morphology changes after plasma treatment. The results are shown in Figure 27. The morphology of the MFC foam prior to plasma treatment remains complex because of its very porous nature (Figure 27A). The mix of fibres combined with leaf-bended structure is clearly visible. The latter is organized with a vertical stack of several sheets, bending over itself, and randomly dispersed throughout the volume. All these sheets remain partially attached to each other owing to a fibrous network. The images obtained at higher magnification (Figures 27B and 27C) highlight the strong anisotropy of the sheets, which have widths of a few hundred micrometres and sub-micrometric thicknesses. The appearance of the microfibres and their sizes are also visible (Figure 27C). These microfibres clearly constitute the base element with which the sheets are formed.

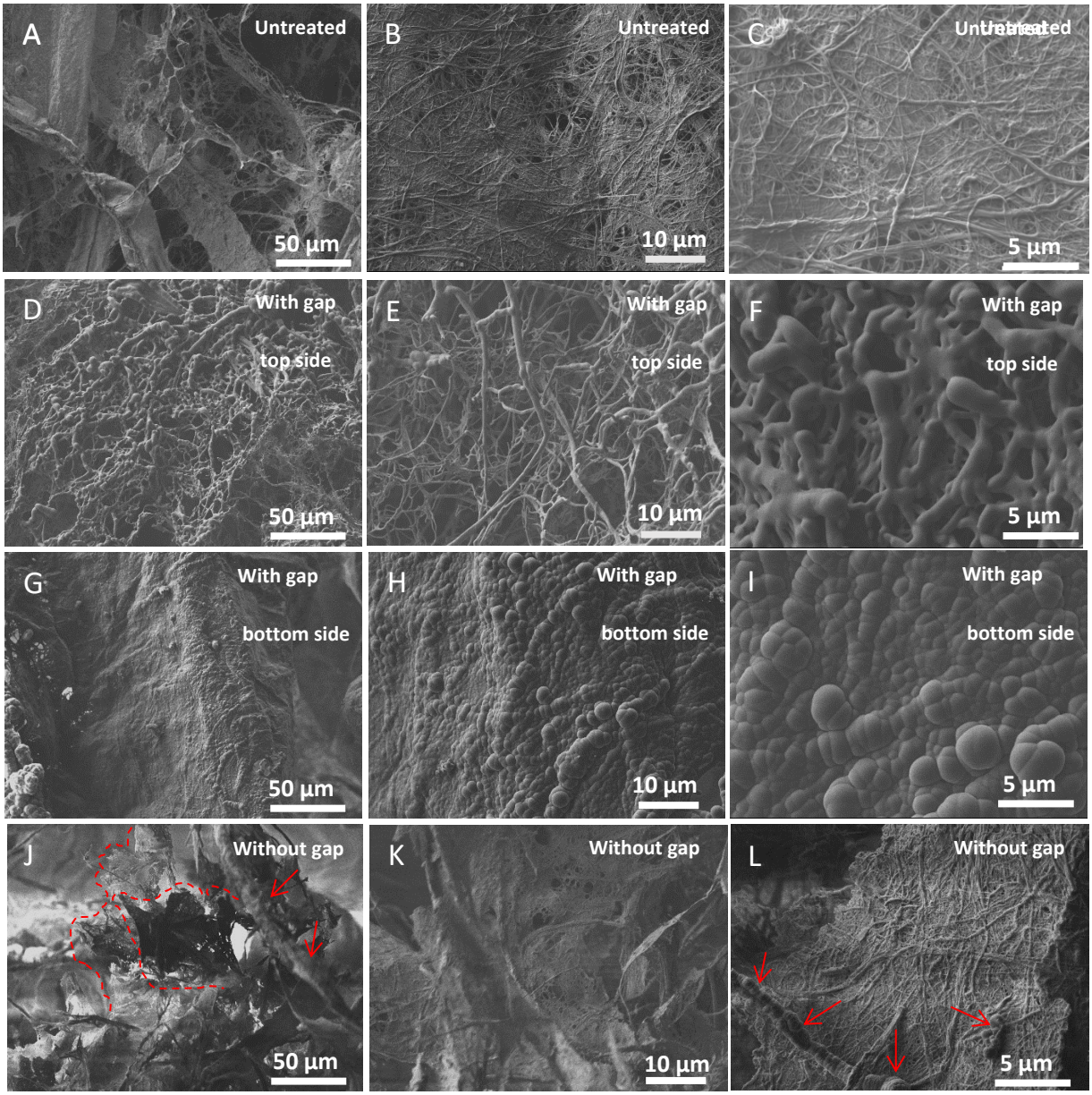

Figure 27. – (A)-(C) SEM images of the untreated MFC foams at different locations for various magnifications: X500 in (A), X2000 in (B) and X5000 in (C). (D)-(F) SEM images of the top side of the plasma-treated MFC foam taking up a portion of the gas gap at different locations for various magnifications: X500 in (D), X2000 in (E) and X5000 in (F). (G)-(I) SEM images of the bottom side of the plasma-treated MFC foam taking up a portion of the gas gap at different locations for various magnifications: X500 in (G), X2000 in (H) and X5000 in (I). (J)-(L) SEM image of the top side of the plasma-treated MFC foam taking up the entirety of the gas gap at different locations for various magnifications: X500 in (J), X2000 in (K) and X5000 in (L).

The morphology of the foam is completely altered once it is subjected to plasma deposition. Figure 27D shows the direct plasma-exposed side of a plasma-treated MFC foam substrate that occupied only a portion of the gas gap volume. The sheet structures are no longer visible and only a very complex fibre network is observed, with fibre dimensions in the 400 nm range (Figures 27E and F). This alteration of the MFC foam can be linked to the direct impingement of energetic species on the topmost surface, including positive helium ions, metastable helium atoms, and ultraviolet photons. The surface of the microfibres does not show the characteristic cauliflower-like morphology obtained with a thin organic layer in DBD [55]. However their typical size in Figure 27F is much higher than before plasma treatment (Figure 27C) because of the material deposition. Due to the highly porous structure observed in Figures 27D-27F, it can be hypothesized that plasma-generated species have the ability to penetrate through the pores of the MFC foam. In this regard, the bottom side of the sample (which was in direct contact with the bottom dielectric plate of the DBD cell) was also analyzed by SEM to verify for any possible alteration and deposition. In contrast to the topmost surface (Figures 27D and 27E), no cellulose defibrillation is observed on the bottom surface (Figures 27G and 27H). In addition, Figure 27I reveals that the cellulosic filaments and microfibres become covered with a dense cauliflower-morphology coating. Hence, significant penetration of plasma-generated species occurs. Other authors have also highlighted the relevant role of diffusive transport through porous cellulosic substrates in non-thermal plasma at atmospheric pressure [69,71].

By comparing the images obtained with a gas gap (configuration A) with those obtained without a gas gap (configuration B), a different result is observed. Figures 27J and 27K indicate that cellulosic sheet structures are still readily visible when no gas gap is present during plasma treatment (no cellulose defibrillation). However, the stained regions reveal localized fragmentation of the sheet structures (see red dotted lines in Figure 27J), while the unstained zones are intact (see Figure 27K). In addition, the “hole” with segmented edges in Figure 27J is of the size of typical discharge filaments (~0.1 mm) [54,99]. Figures 27J to 27L further show that some areas display cauliflower-like aggregates on the fibrillated structures (see red arrows in Figures 27J and 27L) [50,55,69,71], whereas others are not covered with any coating (see

Figure 27K). These results indicate a higher accumulation of deposits in stained zones than in the unstained ones.

3.3.3.3 - Surface Chemical Characterization

In order to correlate the micro- and macroscopic observations obtained from the plasma-treated MFC samples, EDS measurements were carried out. The chemical mappings were recorded near the surface of the MFC foams using a low (5 kV), and high potential (10 kV) to modify the depth of the analysis. Considering the linear chains of cyclic glucose monomers (anhydroglucose rings) composing the MFC substrate as well as the organosilicon compound used as a precursor (HMDSO) during plasma deposition, mostly Si/O and C/O ratios were studied. The surface distribution of the plasma-deposited species is analyzed by chemically mapping the surface (5 measurements were taken for each analysis condition). Figure 28 depicts the ratios obtained by analyzing regions near those imaged by SEM. The expected stochiometric ratio of carbon to oxygen (C/O), determined empirically, is 1.2 for the $(C_6H_{10}O_5)_x$ structure of the cellulosic substrate [6]. To simplify comparisons, this ratio is normalised to 1 in Figure 28. The untreated MFC foam not subjected to any plasma discharge (untreated cellulose) has the same stoichiometric C/O ratio at 5 and 10 kV.

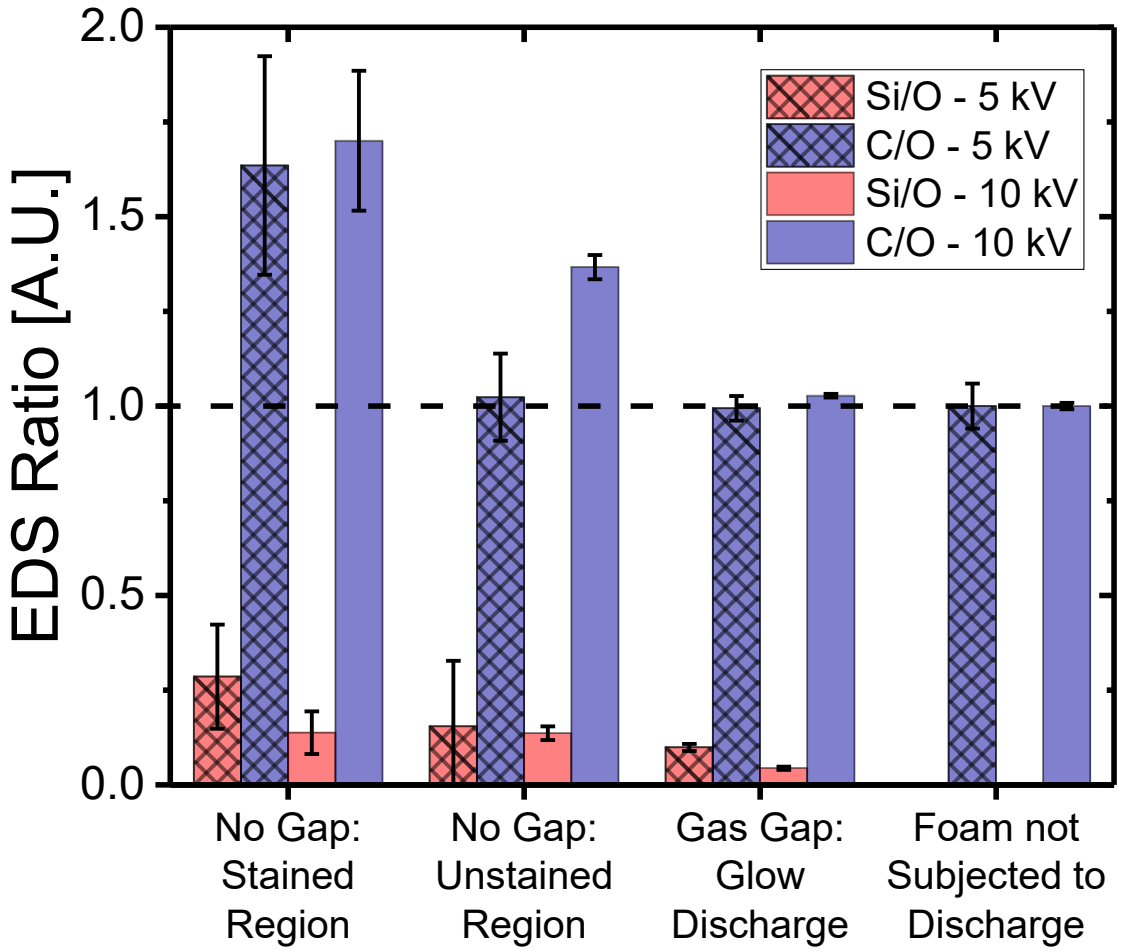

Figure 28. – Mean C/O and Si/O ratios determined through EDS of different MFC foam plasma treatment configurations studied with a dashed line demonstrating the theoretical stoichiometric ratio for C/O (normalised to 1 for simplicity). Error bars indicate the standard deviation of the measurement.

The plasma-treated MFC foam taking up a portion of the gas gap volume had similar C/O ratios to untreated samples. One must note that the precursor (HMDSO) has a stoichiometric ratio of carbon to oxygen of C/O = 6 prior to plasma fragmentation. This means that the deposition of the fragments from HMDSO generates methyl groups on the cellulosic surface and should increases the carbon signature. However, at 5 kV (reduced penetration depth analysis), the standard deviation of the EDS measurements remains small. This indicates that organosilicon deposits did not significantly modify the total amount of carbon per oxygen, and only a thin layer

is deposited even after one hour of plasma treatment. There is a detectable Si/O ratio, confirming the presence of a plasma-deposited coating. The very low standard deviation of these measurements also demonstrates that the coating was homogeneous over the whole surface of the MFC foam. A slightly lower Si/O ratio is observed at 10 kV. This suggests that less coating can be found inside the foam compared to the topmost surface. Similarly, Babaei *et al*. deposited organosilicon coatings on a 4-layer stack of bleached, unrefined Kraft paper [69]. The authors observed that the coating was thicker on the first layer (directly exposed to plasma) compared to the ones underneath.

The analysis at 5 kV of the unstained regions for the MFC foam taking up the entirety of gas gap shows a C/O ratio close to the untreated MFC foam. The C/O values obtained at 10 kV are, however, higher with a smaller standard deviation. Since the MFC foam occupies the entirety of gas gap volume, plasma-generated species most likely travel through the volume of the foam, and not necessarily over its surface. This indicates that most of the reactions occur near the core of the foam, and less on the topmost surface. The Si/O ratios at 5 kV are inhomogeneous and vary from 14% to 0% within a 1 mm^2 area. These large variations in silicon measurements suggest that the coating does not evenly cover the cellulosic surface. In the case of the 10 kV measurements, the ratios have a smaller standard deviation, highlighting the more even chemical distribution inside the foam.

The stained regions of the foam taking up the entirety of the gas gap presented results that differed considerably from the expected values with both penetration analysis conditions. Indeed, consistently high C/O and Si/O ratios are found at every point of these regions. This suggests that the growth rate of the coating is higher in these domains. Thus, the foam taking up only a portion of the gas gap generated very consistent and homogeneous chemical measurements, suggesting a very efficient and widespread coating, both near its surface and within the foam structure. On the other hand, the foam taking up the entirety of gas gap, as stated previously, had yellow discolourations in certain spots on its surface. This indicates preferential

breakdown positions in the filamentary DBD, with enhanced deposition of the organosilicon coating in these domains.

3.3.3.4 - Water Contact Angle Measurements

Figure 29 depicts the water contact angle (WCA) analysis obtained on the plasma-treated MFC foams (all values were recorded 45 s after droplet deposition). Measurements on both the top side and bottom side of the sample have been taken to understand transport and/or precursor penetration through the porous cellulosic substrate. Different measurement points for both plasma treatment configurations are presented: one near the gas entry point, one near the middle of the substrate, and one near the gas exit. For each point, 3 values have been recorded. An absence of error bars (standard deviation) signifies that only a single measurement point returned a non-zero WCA value 45 s after droplet deposition. An absence of measurement means every measurement attempted in that region returned zero WCA values due to complete and rapid absorption of the water droplet. According to literature, the WCA of micro/nano fibrillated cellulosic films and foams is between 15 and 60 degrees [103,104], however, the water droplet settled on the sample is absorbed very quickly (<140 ms), due to the large quantities of OH groups and the highly porous microstructure of these materials [35,36].

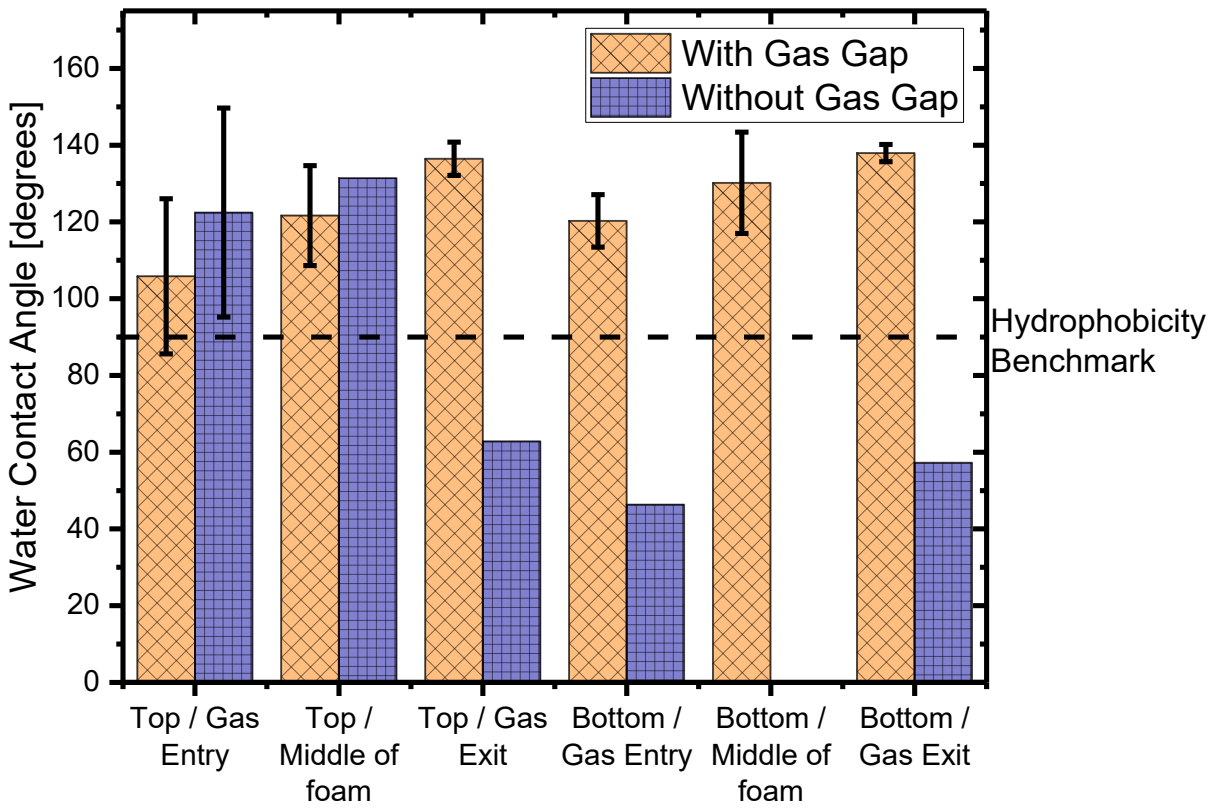

Figure 29. – Mean WCA measurements and standard deviations (Error bars) at the top, and bottom surfaces of the MFC foams measured near the gas entry, the middle of the foam, and the gas exit. All values were recorded 45 s after droplet deposition. Data are shown for foam taking up a portion, and the entirety of the gas gap volume.

Comparing the top and bottom sides of the plasma-treated MFC foam taking up a portion of the gas gap (orange bars), one can note similar water repellency. However, less consistent readings, represented by relatively high standard deviations, have been found in the top layer. Considering the very high porosity of the MFC foams, the high flow rate (4.5 SLM) in the gas gap, as well as the long plasma treatment time (1 h), a low transport of reactive species through the volume of the foam is expected. However, the hydrophobic WCA values on the top and bottom of the foam highlight the high penetration of the discharge treatment within the foam and confirm previous EDS measurements and SEM images. A similar phenomenon has been observed by Mukhopadhyay *et al.* who modified cellulosic sheets with porous microstructure [105]. In their

work, a stack of multiple sheets was treated to enhance their hydrophobicity and the modification throughout different layers was studied. The authors found treatment time to be the most important factor influencing the degree of penetration of plasma-generated species into the substrate [105]. A similar effect has also been observed by Wang *et al.*, who correlated large pore sizes to enhanced penetration into the substrate [65].

WCA values on the MFC foam taking up a portion of the gas gap (orange bars) are consistently less hydrophobic near the gas entry than near the gas exit, regardless of orientation of the foam. For example, the WCA value near the gas entry on the top of the foam is 105 ± 20 degrees, whereas it is 137 ± 4 degrees near the gas exit. The standard deviations for these values show that the homogeneity of plasma treatment remains higher near the exit. The variation between the entry and exit is attributed to the modification of the coating thickness and/or the differentiation of chemical groups. Indeed, it was expected to find a modification of the coating properties (*i.e*. thickness and hydrophobicity) depending on the surface position with respect to the discharge entrance [67,69]. This is attributed to four phenomena: the gradual longitudinal consumption of precursor molecules, the penetration of the plasma-generated species inside the substrate volume, the substrate outgassing, and the modification of density and temperature of energetic species involved in precursor fragmentation and plasma deposition [67]. The latter depends mainly on residence time in the discharge and the power-to-precursor concentration ratio [69]. It was also demonstrated by Xu *et al.* that coating thickness and surface roughness had a direct impact on hydrophobicity measurements [106].

Figure 30 presents the WCA and water droplet volume versus time after droplet deposition for the plasma-treated sample taking up a portion of the gas gap. As can be seen in Figure 30, the rate of decrease of the WCA and water droplet volume for the plasma-treated sample is relatively small. The same measurements were recorded for a silicon wafer exposed to comparable experimental conditions [69]. Comparing the rate of change in the volume of the water droplet on plasma-treated foam and silicon samples supports the fact that the decrease in

the droplet volume settled on the plasma deposited paper originates mostly from evaporation rather than adsorption or penetration.

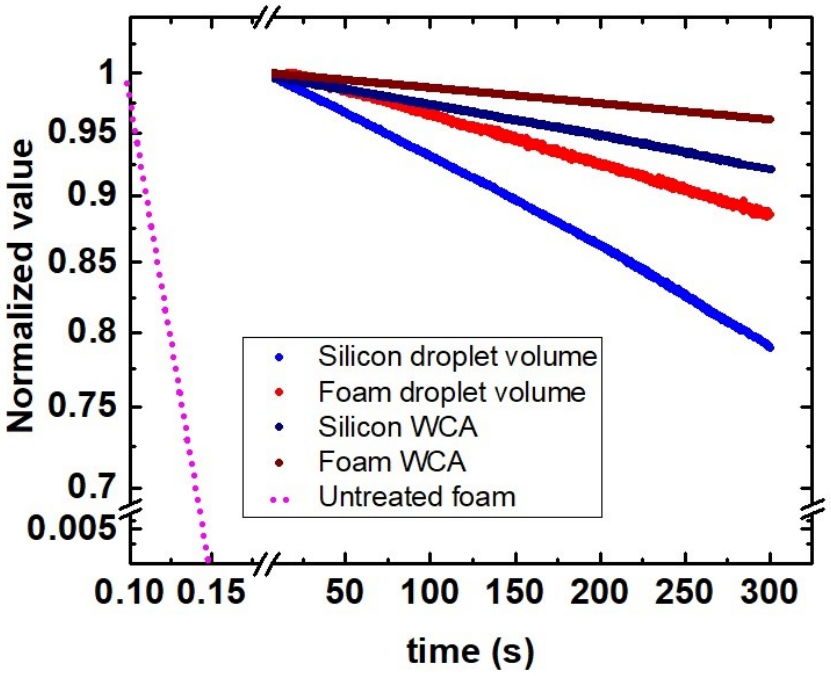

Figure 30. – The change of normalized water contact angle and water droplet volume (normalized to initial measurement value) over time after water droplet on a plasma-treated MFC foam (taking up a portion of the gas gap volume) and a plasma-treated silicon. The volume of water droplet settled on an untreated foam was also shown for comparison.

Figure 29 also presents WCA measurements when the MFC foam occupies the entirety of the gas gap volume (blue bars). For these conditions, one can readily observe the inhomogeneity in WCA values across the sample. Indeed, as explained in section 3.2, localized treatments are produced throughout the discharge. Previous work has demonstrated that this phenomenon consistently occurs in the same surface region as treatment time continues [98], increasing the inhomogeneity on both the bottom and top sides of the foam. This is associated with the presence of some hydrophilic regions (WCA <90 degrees [106–109]). As an example, the WCA value of the top layer is 62 degrees at the exit (whereas it is 122 ± 27 degrees at the entrance). This is even more evident on the bottom of the MFC foams where measurements are consistently lower than

the top side. The dependence of the water droplet absorption on the position of the gas entrance on the sample obtained without gas gap demonstrates the poor homogeneity of the plasma treatment. The difference observed between the top and bottom surfaces indicate a significant loss of the reactive species close to the stained regions [106,108,109]. Therefore, hydrophobic coating is significantly improved when MFC foams take up only a portion of the gas gap volume as opposed to the entirety of the gas gap volume.

3.3.3.5 - Oleophilicity Measurements

To gain insight into the potential of selective adsorption properties of the MFC foams after plasma treatment, contact angle measurements with water and kerosene were compared. The results are shown in Figure 31. The droplets (5 µL) are deposited at the surface (entrance of the discharge) and recorded over a few minutes. Based on the previous analysis results, the oleophilic *vs.* hydrophobic properties were measured only on the MFC foam that took up a portion of gas gap volume to ensure analysis on homogeneous coatings. The behaviour of untreated MFC foams with kerosene/water is also presented. When untreated, the foam exhibits strong absorbance characteristics. Indeed, the water and the kerosene droplets are absorbed within 140 ms (see Figures 31A and 31B). This means that untreated MFC foams exhibit not only very hydrophilic properties but also very oleophilic behaviour. Therefore, due to absorbing water and oil at the same time, the cellulosic foam in their pristine form is not desired for decontamination of oily wastewater. To gain an insight into the properties of the foams throughout their volume, both the top and bottom of the foams were analyzed. On the foam's top side (see Figure 31C), a 107-degree WCA is measured. A kerosene droplet is then manually added in close vicinity to the water droplet and is absorbed within 140 ms. A similar behaviour was found on the bottom side of the plasma-treated MFC foam taking up a portion of the gas gap (see Figure 31D).

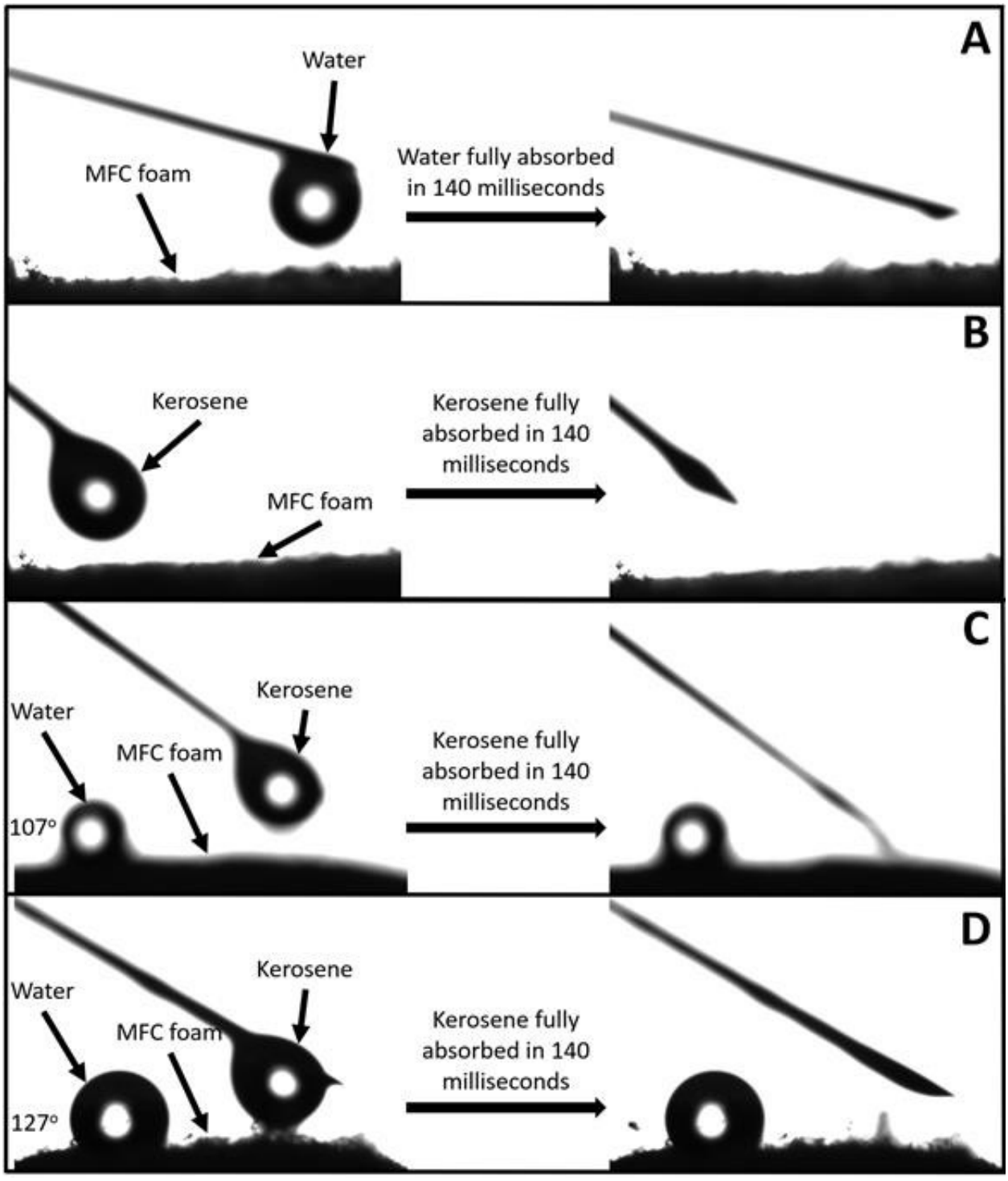

Figure 31. – Interaction of untreated MFC foam with either (A) water or (B) kerosene. Interaction of plasma-treated MFC foam (taking up a portion of the gas gap volume) with water and kerosene on (C) the top side and (D) the bottom side of the MFC foam.

The images presented in Figure 31 demonstrate that plasma treatment of MFC foams with a gas gap produces a very homogeneous selective coating over the entire surface and volume. These results are akin to oleophilicity, as the plasma-treated MFC foams readily and immediately absorb the kerosene while repelling water. Similarly, Mansourizadeh *et al.* also treated a polyethersulfone/cellulose membrane for oil-water separation [57]. Rohrbach *et al.* similarly increased the hydrophilicity and oleophobicity of a hydrated regular cellulose paper filter [59]. These works, along with the results obtained in this paper, are promising steps towards the use of sustainable woody biomass-derived polymers in the effective treatment and decontamination of waterways polluted by oily substrates. This, in turn, could successfully reduce the carbon footprints of many industries through judicious functionalization of these biomaterials.

3.3.4 - Conclusion

An atmospheric-pressure helium dielectric barrier discharge with hexamethyldisiloxane was used to confer hydrophobic properties to microfibrillated cellulosic foams without altering their oleophilic properties. Two different experimental configurations were examined, one where the foams took up the entirety of the gas gap volume, and another where the foams took up only a portion of the gas gap volume. It was found that a highly energetic filamentary discharge regime was prioritized when foams took up the entirety of gas gap volume. This generated damage on the foam's surface and within its volume in the form of burns. When the foams took up only a portion of the gas gap volume, it was found that the discharge regime was glow-like and produced some cellulose defibrillation on the topmost surface with no significant damage on the bottom surface. Foams taking up all of gas gap produced discoloured, yellowed regions on their surfaces post plasma treatment, while foams taking up a portion of the gas gap always retained their initial pristine white colour post plasma treatment. This demonstrates that plasma treatment on the MFC foams taking up the entirety of the gas gap was very inefficient with random and highly localized deposits. In line with the above-mentioned observations, the MFC foam taking up a portion of the gas gap also showed a consistent hydrophobic behaviour on both the top and bottom surfaces. Olephilicity measurements with kerosene, however, found that the foam was

very oleophilic and remained oleophilic even after plasma deposition, independent of configuration. This further suggests that the plasma-treated foam had selective adsorption properties. The results from this work distinctly demonstrate that plasma modification of cellulosic (MFC) foams is most effective when carried out using a configuration in which a gas gap is present.

Overall, the findings of this study reveal that the plasma-deposited MFC foams can be potentially implemented in decontamination of oily wastewater using renewable and sustainable cellulosic materials. However, the fragile structure of the MFC foams could limit their use in industrial applications. A reinforcing of their structure could catapult these foams to the forefront of the future's green and applicable technologies.

3.3.5 - Acknowledgments

This work was financially supported by the National Science and Engineering Research Council (NSERC), PRIMA-Québec, Plasmionique Inc., FPInnovations, and the Centre Collégial de Transfert de Technologie (CCTT) through the Fonds de Recherche Québécoise en Nature et Technologies (FRQNT). Louis-Félix Meunier acknowledges Mitacs Globalink, the Direction des Relations Internationales of the Université de Montréal and Université Paul-Sabatier de Toulouse for their support to the Québec-France student exchange master program.

Chapter 4 – Conclusion and perspectives

The main objective of this work was to examine the fundamental discharge characteristics occurring in an atmospheric pressure dielectric barrier discharge in the presence of a microfibrillated cellulosic (MFC) foam taking up both a portion of gas gap volume and the entirety of gas gap volume. To explore potential valorisation of these foams, hexamethyldisiloxane precursor was used to confer hydrophobic properties to the MFC foams by plasma deposition of organosilicon coatings all the while maintaining the foam's characteristic oleophilicity.

Initially, two different frequencies were analysed in similar empirical conditions. MFC foams, some outgassed, and some not outgassed, all occupying the entirety of gas gap volume were subjected to two different frequencies: 10 kHz and 60 kHz. Electrical measurements combined with fast optical imaging studies were made to acquire a qualitative understanding of the discharge properties. It was discovered that discharge ignition and its ultimate propagation occurred primarily through the volume of the foam from one electrode to the other (volume discharge). Higher frequency measurements done at 60 kHz generated a higher power output, directly contributing to greater amounts of damages incurred by the foams than the damages observed at 10 kHz. Ultimately, a higher frequency measurement generated higher amounts of volumetric damage. It was found that outgassing the MFC foams prior to subjecting them to a plasma discharge greatly reduced the power output of the discharge, in turn reducing the amount of damage incurred to the foams. It was concluded that the gradual release of oxidising species issued from ambient air initially trapped in the foam during the discharge (outgassing) contributed to a reaction environment with higher amounts of impurities. This directly increased power output, contributing to surface damages. When MFC foams were fully outgassed prior to plasma ignition, electrical and optical measurements revealed a homogeneous glow-like discharge regime at 60 kHz and a filamentary-like discharge regime at 10 kHz, with significantly reduced damages than in non-outgassed conditions.

The previous measurements were then utilised to increase the potential functionalities of the MFC foams studied in this work. Indeed, the foams have a naturally high hydrophilicity and oleophilicity. Plasma modification was done to alter their reaction with water, ultimately rendering them hydrophobic, all the while retaining their characteristic oleophilicity. In similar fashion, the foams were subjected to an atmospheric pressure dielectric barrier discharge in helium but with added HMDSO as a precursor gas for plasma deposition. This allowed the production of a coating producing hydrophobic properties without any alteration of the oleophilic characteristics. Two different experimental configurations were examined, one where the MFC foams occupied the entirety of gas gap volume and one where they occupied only a portion of gas gap volume. Everything else was kept identical. It was discovered that highly energetic filamentary discharges were produced when foams took up the entirety of gas gap volume. This, in turn, generated high amounts of damage on the MFC foam's surface and volume, taking the form of burns. When foams took up only a portion of gas gap volume as opposed to its entirety, the discharge regime transitioned to a homogeneous glow-like discharge. This also generated cellulose defibrillation on the foam's top-most surface at the microscopic level. No significant damage was incurred by the foam's bottom surface. Foams taking up all of gas gap volume produced discoloured, yellowed regions on their surfaces post plasma treatment. These discolourations are believed to be sourced from randomly distributed, highly intense, inhomogeneous deposits from the HMDSO precursor molecules on the foam's surface. The MFC foam occupying only a portion of gas gap volume did not generate these discolourations, and instead produced a homogeneous coating from the HMDSO precursor molecule. This allowed for a hydrophobic surface on both the top and bottom surfaces of the MFC foam. Oleophilicity measurements were also done using kerosene. Despite plasma treatment, MFC foams retained their very oleophilic nature. This suggests that the plasma-treated foam developed selective adsorption properties. This demonstrates that the plasma modification of cellulosic (MFC) foams is most effective when carried out using a configuration in which a gas gap is present.

Ultimately, this work has brought forth the possibility of modifying bio-degradable, bio-compatible, eco-friendly, green, microfibrillated cellulosic (MFC) foams through plasma processing. One of the leading potential uses of these foams could be through its unique hydrophobic and oleophilic properties conferred through the deposition of organo-silicon functional groups issued from the non-toxic HMDSO precursor using atmospheric pressure DBDs. For instance, the low degradability of oily products in nature, as well as their toxic composition, can strongly affect our biosphere, doubly so if mixed with water. Oily wastewater is currently a great source of water stream contamination. It could be possible to decontaminate oily wastewater using renewable and sustainable cellulosic materials combined with green and eco-friendly plasma processes.

Références bibliographiques

[1] N. Naudé, *Étude Électrique de La Physique d'une Décharge de Townsend à La Pression Atmosphérique et de Son Interaction Avec Un Générateur: Modèle et Expérience* (Toulouse, 2005).

[2] F. Massines, C. Sarra-Bournet, F. Fanelli, N. Naudé, and N. Gherardi, Plasma Process. Polym. **9**, 1041 (2012).

[3] N. Naudé, J. Paillol, A. Belinger, and R. Subileau, in *Mission Ressources Compétences Technol.* (2012), pp. 229–238.

[4] M. J. Druyvesteyn and F. M. Penning, Rev. Mod. Phys. **12**, 87 (1940).

[5] L. Brinchi, F. Cotana, E. Fortunati, and J. M. Kenny, Carbohydr. Polym. **94**, 154 (2013).

[6] R. J. Moon, A. Martini, J. Nairn, J. Simonsen, and J. Youngblood, Chem. Soc. Rev. **40**, 3941 (2011).

[7] D. Klemm, B. Heublein, H. P. Fink, and A. Bohn, Angew. Chemie - Int. Ed. **44**, 3358 (2005).

[8] M. Isik, H. Sardon, and D. Mecerreyes, Int. J. Mol. Sci. **15**, 11922 (2014).

[9] C. F. Cross, E. J. Bevan, and C. Beadle, J. Chem. Soc. Trans. **63**, 167 (1893).

[10] F. Massines, N. Gherardi, N. Naudé, and P. Ségur, EPJ Appl. Phys. **47**, 22805 (2009).

[11] M. Baiardo, G. Frisoni, M. Scandola, and A. Licciardello, J. Appl. Polym. Sci. **83**, 38 (2002).

[12] G. Rodionova, M. Lenes, Ø. Eriksen, and Ø. Gregersen, Cellulose **18**, 127 (2011).

[13] C. Yin, J. Li, Q. Xu, Q. Peng, Y. Liu, and X. Shen, Carbohydr. Polym. **67**, 147 (2007).

[14] J. Profili, S. Asadollahi, P. Vinchon, A. Dorris, S. Beck, A. Sarkassian, and L. Stafford, Prog. Org. Coatings **147**, 105865 (2020).

[15] S. Maiti, I. M. Mishra, S. D. Bhattacharya, and J. K. Joshi, Colloids Surfaces A Physicochem. Eng. Asp. **389**, 291 (2011).

[16] R. Gao, Q. Liu, J. Wang, J. Liu, W. Yang, Z. Gao, and L. Liu, Appl. Surf. Sci. **289**, 417 (2014).

[17] Government of Canada, *Wastewater Systems Effluent Regulations: SOR/2012-139. Règlement Sur Les Effluents Des Systèmes d ' Assainissement Des Eaux Usées: DORS/2012-139* (Ottawa, Canada, 2016).

[18] A. A. Al-Shamrani, A. James, and H. Xiao, Water Res. **36**, 1503 (2002).

[19] J. Yang, Y. Tang, J. Xu, B. Chen, H. Tang, and C. Li, Surf. Coatings Technol. **272**, 285 (2015).

[20] A. B. Nordvik, J. L. Simmons, K. R. Bitting, A. Lewis, and T. Strøm-Kristiansen, Spill Sci. Technol. Bull. **3**, 107 (1996).

[21] J. An, J. F. Cui, Z. Q. Zhu, W. D. Liang, C. J. Pei, H. X. Sun, B. P. Yang, and A. Li, J. Appl. Polym. Sci. **131**, 9197 (2014).

[22] P. Brunet, Procédé de Dépôt de Couches Minces Nanocomposites Par Décharge à Barrière Diélectrique: De l'aérosol d'une Suspension Colloïdale à La Morphologie Du Dépôt, Université de Perpignan Via Domitia, 2017.

[23] P. Brunet, R. Rincón, J. M. Martinez, Z. Matouk, F. Fanelli, M. Chaker, and F. Massines, Plasma Process. Polym. **14**, 1700049 (2017).

[24] J. Felix, P. Gatenholm, and H. P. Schreiber, J. Appl. Polym. Sci. **51**, 285 (1994).

[25] J. Shi, L. Lu, W. Guo, Y. Sun, and Y. Cao, J. Appl. Polym. Sci. **130**, 3652 (2013).

[26] J. Morales, M. G. Olayo, G. J. Cruz, P. Herrera-Franco, and R. Olayo, J. Appl. Polym. Sci. **101**, 3821 (2006).

[27] F. Poncin-Epaillard, G. Legeay, and J. -C Brosse, J. Appl. Polym. Sci. **44**, 1513 (1992).

[28] J. Profili, S. Rousselot, E. Tomassi, E. Briqueleur, D. Aymé-Perrot, and M. Stafford, Luc, Dollé, Am. Chem. Soc. **8**, 4728 (2020).

[29] U. Kogelschats, B. Eliasson, and W. Egli, Phys IV Fr. **7**, 47 (1997).

[30] D. Merche, N. Vandencasteele, and F. Reniers, Thin Solid Films **520**, 4219 (2012).

[31] G. Borcia, C. A. Anderson, and N. M. D. Brown, Surf. Coatings Technol. **201**, 3074 (2006).

[32] O. Levasseur, R. Kumar Gangwar, J. Profili, N. Naudé, N. Gherardi, and L. Stafford, Plasma Process. Polym. **14**, 1600172 (2017).

[33] O. Levasseur, J. Profili, R. K. Gangwar, N. Naudé, R. Clergereaux, N. Gherardi, and L. Stafford, Plasma Sources Sci. Technol. **23**, 054006 (2014).

[34] R. K. Gangwar, O. Levasseur, N. Naudé, N. Gherardi, F. Massines, J. Margot, and L. Stafford, Plasma Sources Sci. Technol. **25**, 015011 (2015).

[35] J. Prégent, L. Vandsburger, V. Blanchard, P. Blanchet, B. Riedl, A. Sarkissian, and L. Stafford, Cellulose **22**, 3397 (2015).

[36] J. Prégent, L. Vandsburger, V. Blanchard, P. Blanchet, B. Riedl, A. Sarkissian, and L. Stafford, Cellulose **22**, 811 (2015).

[37] J. P. Borra, J. Phys. D. Appl. Phys. **39**, R19 (2006).

[38] R. Morent, N. De Geyter, J. Verschuren, K. De Clerck, P. Kiekens, and C. Leys, Surf. Coatings Technol. **202**, 3427 (2008).

[39] F. Massines, P. Ségur, N. Gherardi, C. Khamphan, and A. Ricard, Surf. Coatings Technol. **8**, 8 (2003).

[40] Z. Navrátil, R. Brandenburg, D. Trunec, A. Brablec, P. Sťahel, H. E. Wagner, and Z. Kopecký, Plasma Sources Sci. Technol. **15**, 8 (2006).

[41] L. Mangolini, C. Anderson, J. Heberlein, and U. Kortshagen, J. Phys. D. Appl. Phys. **37**, 1021 (2004).

[42] D. Trunec, Z. Navrátil, P. Sťahel, L. Zajíčková, V. Buršíková, and J. Ćech, J. Phys. D. Appl. Phys. **37**, 2112 (2004).

[43] N. Naudé, Etude Électrique de La Physique d ' Une Décharge de Townsend à La Pression Atmosphérique et de Son Interaction Avec Un Générateur : Modèle et Expérience To Cite This Version : HAL Id : Tel-00601053, Université Toulouse III - Paul Sabatier, 2011.

[44] N. Naudé, J. P. Cambronne, N. Gherardi, and F. Massines, J. Phys. D. Appl. Phys. **38**, 530 (2005).

[45] N. Gherardi and F. Massines, IEEE Trans. Plasma Sci. **29**, 536 (2001).

[46] F. Massines, N. Gherardi, N. Naudé, and P. Ségur, Plasma Phys. Control. Fusion **47**, B577 (2005).

[47] X. C. Li, L. F. Dong, and L. Wang, Chinese Phys. **14**, 1418 (2005).

[48] N. Naudé and F. Massines, IEEE Trans. Plasma Sci. **36**, 1322 (2008).

[49] O. Levasseur, L. Stafford, N. Gherardi, N. Naudé, E. Beche, J. Esvan, P. Blanchet, B. Riedl, and A. Sarkissian, Surf. Coatings Technol. **234**, 42 (2013).

[50] O. Levasseur, L. Stafford, N. Gherardi, N. Naudé, V. Blanchard, P. Blanchet, B. Riedl, and A. Sarkissian, Plasma Process. Polym. **9**, 1168 (2012).

[51] F. Massines, N. Gherardi, A. Fornelli, and S. Martin, Surf. Coatings Technol. **200**, 1855 (2005).

[52] S. Soulié, Étude de l'asclépiade Pour Des Applications de Regénération Osseuses, Université Laval, 2018.

[53] U. Kogelschatz, IEEE Trans. Plasma Sci. **30**, 1400 (2002).

[54] Ulrich Kogelschatz, Plasma Chem. Plasma Process. **23**, 1 (2003).

[55] J. Profili, O. Levasseur, A. Koronai, L. Stafford, and N. Gherardi, Surf. Coatings Technol. **309**, 729 (2017).

[56] O. Levasseur, Exam. Général Pré-Doctoral (2013).

[57] A. Mansourizadeh and A. Javadi Azad, J. Polym. Res. **21**, 375 (2014).

[58] A. Srinivasan and T. Viraraghavan, J. Hazard. Mater. **175**, 695 (2010).

[59] K. Rohrbach, Y. Li, H. Zhu, Z. Liu, J. Dai, J. Andreasen, and L. Hu, Chem. Commun. **50**, 13296 (2014).

[60] G. Wang, Y. He, H. Wang, L. Zhang, Q. Yu, S. Peng, X. Wu, T. Ren, Z. Zeng, and Q. Xue, Green Chem. **17**, 3093 (2015).

[61] A. Fateev, F. Leipold, Y. Kusano, B. Stenum, E. Tsakadze, and H. Bindslev, Plasma Process. Polym. **2**, 193 (2005).

[62] C. X. Wang, Y. Liu, H. L. Xu, Y. Ren, and Y. P. Qiu, Appl. Surf. Sci. **254**, 2499 (2008).

[63] R. Morent, N. De Geyter, L. Gengembre, C. Leys, E. Payen, S. Van Vlierberghe, and E. Schacht, Eur. Phys. J. Appl. Phys. **43**, 289 (2008).

[64] H. U. Poll, U. Schladitz, and S. Schreiter, Surf. Coatings Technol. **142**, 489 (2001).

[65] C. X. Wang, Y. Ren, and Y. P. Qiu, Surf. Coatings Technol. **202**, 77 (2007).

[66] C. X. Wang and Y. P. Qiu, Surf. Coatings Technol. **201**, 6273 (2007).

[67] I. Enache, H. Caquineau, N. Gherardi, T. Paulmier, L. Maechler, and F. Massines, Plasma Process. Polym. **4**, 806 (2007).

[68] S. Förster, C. Mohr, and W. Viöl, Surf. Coatings Technol. **200**, 827 (2005).

[69] S. Babaei, J. Profili, A. Dorris, S. Beck, A. Sarkassian, and L. Stafford, Plasma Process. Polym. **Early View**, e2000091 (2020).

[70] European Union, (2019).

[71] J. Profili, S. Asadollahi, P. Vinchon, A. Dorris, S. Beck, A. Sarkassian, and L. Stafford, Prog. Org. Coatings **147**, 105865 (2020).

[72] P. Brunet, R. Rincón, Z. Matouk, M. Chaker, and F. Massines, Langmuir **34**, 1865 (2018).

[73] F. Fanelli and F. Fracassi, Plasma Process. Polym. **13**, 470 (2016).

[74] S. M. Mukhopadhyay, R. V. Pulikollu, and A. K. Roy, Appl. Surf. Sci. **225**, 223 (2004).

[75] S. E. Alexandrov, N. McSporran, and M. L. Hitchman, Chem. Vap. Depos. **11**, 481 (2005).

[76] V. Armenis, F. Fanelli, and F. Fracassi, in *IEEE Nanotechnol. Mater. Devices Conf.* (2016).

[77] F. Massines, P. Ségur, N. Gherardi, C. Khamphan, and A. Ricard, Surf. Coatings Technol. **174**–**175**, 8 (2003).

[78] F. Fanelli, P. Bosso, A. M. Mastrangelo, and F. Fracassi, Jpn. J. Appl. Phys. (2016).

[79] L. C. Vander Wielen, M. Östenson, P. Gatenholm, and A. J. Ragauskas, Carbohydr. Polym. **65**, 179 (2006).

[80] C. N. Flynn, C. P. Byrne, and B. J. Meenan, Surf. Coatings Technol. **233**, 108 (2013).

[81] Y. Kusano, B. Madsen, L. Berglund, and K. Oksman, Cellulose **26**, 7185 (2019).

[82] O. Levasseur, J. Profili, R. K. Gangwar, N. Naudé, R. Clergereaux, N. Gherardi, and L. Stafford, Plasma Sources Sci. Technol. **23**, 054006 (2014).

[83] M. H. Asghar, F. Placido, and S. Naseem, Eur. Phys. JournalApplied Phys. **184**, 177 (2006).

[84] N. Naude and F. Massines, IEEE Trans. Plasma Sci. **36**, 1322 (2008).

[85] V. Pellerin-Boudriau, J.-S. Boisvert, P.-G. Rozon, F. Montpetit, and L. Stafford, Plasma Sources Sci. Technol. **28**, 085011 (2019).

[86] J.-S. Boisvert, L. Stafford, N. Naudé, J. Margot, and F. Massines, Plasma Sources Sci. Technol. **27**, 035005 (2018).

[87] O. Levasseur, A. Bouarouri, N. Naudé, R. Clergereaux, N. Gherardi, and L. Stafford, IEEE Trans. Plasma Sci. **42**, (2014).

[88] R. Brandenburg, Plasma Sources Sci. Technol. **26**, 053001 (2017).

[89] J. Prégent, G. Robert-Bigras, and L. Stafford, Plasma Process. Polym. **15**, e1800035 (2018).

[90] L. Xu, N. Liu, Y. Cao, F. Lu, Y. Chen, X. Zhang, L. Feng, and Y. Wei, ACS Appl. Mater. Interfaces **6**, 13324 (2014).

[91] D. D. La, T. A. Nguyen, S. Lee, J. W. Kim, and Y. S. Kim, Appl. Surf. Sci. **257**, 5705 (2011).

[92] Q. Chen, A. De Leon, and R. C. Advincula, ACS Appl. Mater. Interfaces **7**, 18566 (2015).

[93] B. Akhavan, K. Jarvis, and P. Majewski, ACS Appl. Mater. Interfaces **5**, 8563 (2013).

[94] G. Deschamps, H. Caruel, M. E. Borredon, C. Albasi, J. P. Riba, C. Bonnin, and C. Vignoles, Environ. Sci. Technol. **37**, 5034 (2003).

[95] E. R. P. Keijsers, G. Yilmaz, and J. E. G. Van Dam, Carbohydr. Polym. **93**, 9 (2013).

[96] R. Lu, Y. Yu, G. Adkhamjon, W. Gong, X. Sun, and L. Liu, Cellulose **27**, 7283 (2020).

[97] T. Shao, C. Zhang, K. Long, D. Zhang, J. Wang, P. Yan, and Y. Zhou, Appl. Surf. Sci. **256**, 3888 (2010).

[98] L.-F. Meunier, J. Profili, S. Babaei, N. Naudé, and L. Stafford, Plasma Sources Sci. Technol. (2020).

[99] O. Levasseur, M. Vlad, J. Profili, N. Gherardi, A. Sarkissian, and L. Stafford, Wood Sci. Technol. **51**, 1339 (2017).

[100] M. J. P. Macedo, G. S. Silva, M. C. Feitor, T. H. C. Costa, E. N. Ito, and J. D. D. Melo, J. Mater. Res. Technol. **9**, 2467 (2019).

[101] J. Garcia-Torres, D. Sylla, L. Molina, E. Crespo, J. Mota, and L. Bautista, Appl. Surf. Sci. **305**, 292 (2014).

[102] L.-F. Meunier, J. Profili, S. Babaei, S. Asadollahi, A. Sarkissian, A. Dorris, S. Beck, N. Naudé, and L. Stafford, Plasma Sources Sci. Technol. (2020).

[103] D. Pasquini, M. N. Belgacem, A. Gandini, and A. A. da S. Curvelo, J. Colloid Interface Sci. **295**, 79 (2006).

[104] T. A. Dankovich and D. G. Gray, J. Adhes. Sci. Technol. **25**, 699 (2011).

[105] S. M. Mukhopadhyay, P. Joshi, S. Datta, J. G. Zhao, and P. France, J. Phys. D. Appl. Phys. **35**, 1927 (2002).

[106] Z. W. Xu, Y. K. Zhang, T. H. Chen, J. H. Chang, T. H. Lee, P. Y. Li, and D. S. Liu, Materials (Basel). **11**, 1089 (2018).

[107] I. R. Durán and G. Laroche, Prog. Mater. Sci. **99**, 106 (2019).

[108] I. R. Durán and G. Laroche, Adv. Colloid Interface Sci. **263**, 68 (2019).

[109] N. Agam and P. R. Berliner, J. Arid Environ. **65**, 572 (2006).